

Sleep Neurophysiological Dynamics Through the Lens of Multitaper Spectral Analysis

During sleep, cortical and subcortical structures within the brain engage in highly structured oscillatory dynamics that can be observed in the electroencephalogram (EEG). The ability to accurately describe changes in sleep state from these oscillations has thus been a major goal of sleep medicine. While numerous studies over the past 50 years have shown sleep to be a continuous, multifocal, dynamic process, long-standing clinical practice categorizes sleep EEG into discrete stages through visual inspection of 30-s epochs. By representing sleep as a coarsely discretized progression of stages, vital neurophysiological information on the dynamic interplay between sleep and arousal is lost. However, by using principled time-frequency spectral analysis methods, the rich dynamics of the sleep EEG are immediately visible—elegantly depicted and quantified at time scales ranging from a full night down to individual microevents. In this paper, we review the neurophysiology of sleep through this lens of dynamic spectral analysis. We begin by reviewing spectral estimation techniques traditionally used in sleep EEG analysis and introduce multitaper spectral analysis, a method that makes EEG spectral estimates clearer and more accurate than traditional approaches. Through the lens of the multitaper spectrogram, we review the oscillations and mechanisms underlying the traditional sleep stages. In doing so, we will demonstrate how multitaper spectral analysis makes the oscillatory structure of traditional sleep states instantaneously visible, closely paralleling the traditional hypnogram, but with a richness of information that suggests novel insights into the neural mechanisms of sleep, as well as novel clinical and research applications.

The Discretization of Sleep

Since the first recordings of the electroencephalogram (EEG), scientists have sought to characterize the complex recurring patterns of neural activity observed over many hours during sleep. Primarily, these patterns have been organized through the process of sleep staging, which breaks the sleep continuum into a set of discrete stages using a rule-based categorization of sleep. These stages are defined through visual inspection of the sleep EEG and other physiological waveforms in discrete 30-s epochs, or time windows (FIGURE 1A). The resulting progression of sleep stages as a function of time is called a

Michael J. Prerau,¹ Ritchie E. Brown,²
Matt T. Bianchi,³
Jeffrey M. Ellenbogen,⁴ and
Patrick L. Purdon¹

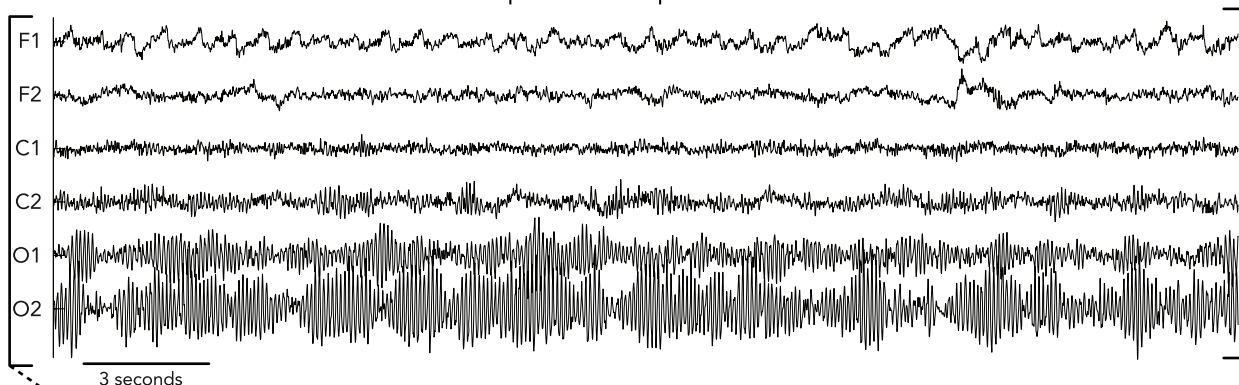
¹Department of Anesthesia, Critical Care, and Pain Medicine, Massachusetts General Hospital, Charlestown, Massachusetts;

²Department of Psychiatry, Laboratory of Neuroscience, VA Boston Healthcare System and Harvard Medical School, Brockton, Massachusetts; ³Department of Neurology, Massachusetts General Hospital, Boston, Massachusetts; and

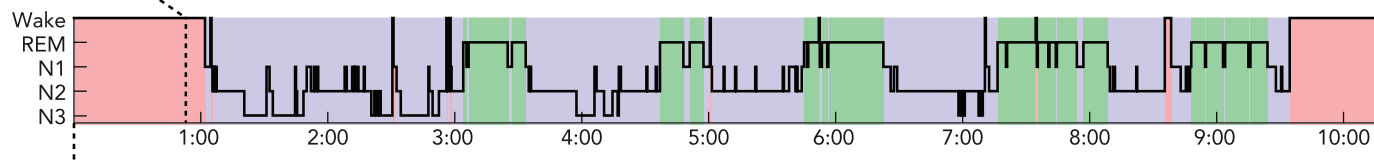
⁴Department of Neurology, Johns Hopkins University, Baltimore, Maryland
prerau@nmr.mgh.harvard.edu
patrickp@nmr.mgh.harvard.edu

A

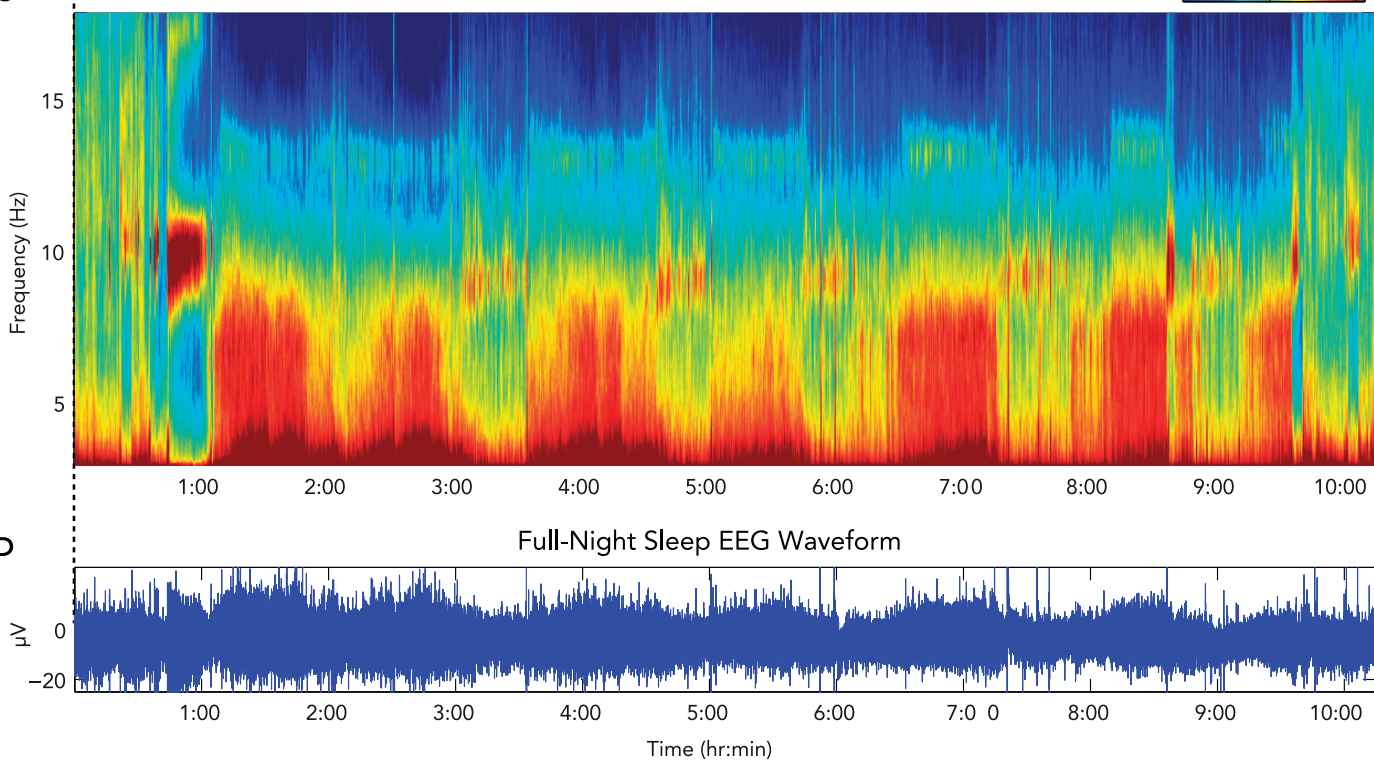
30-Second Epoch of Sleep EEG Waveforms

**B**

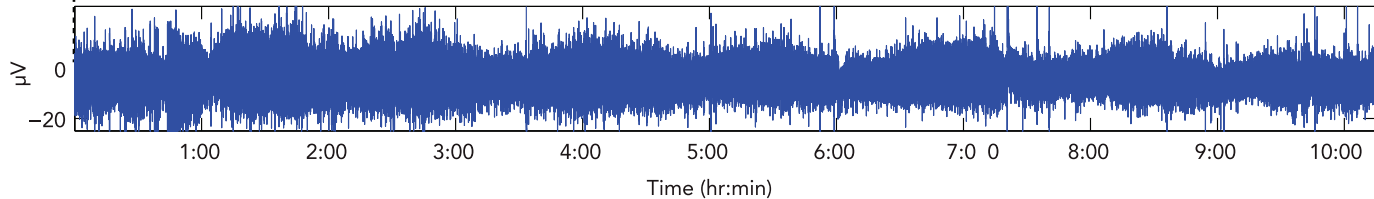
Full-Night Technician-Scored Hypnogram

**C**

Full-Night Sleep EEG Multitaper Spectrogram

**D**

Full-Night Sleep EEG Waveform

**FIGURE 1.** Dynamic spectral analysis of sleep EEG provides a data-rich, high-resolution characterization of neural activity that is more informative than traditional visual sleep staging

In clinical sleep polysomnography (PSG), EEG waveforms (A) from bilateral frontal (F1, F2), central (C1, C2), and occipital (O1, O2) electrodes are recorded along with other physiological signals. These signals are then visually scored by technicians who painstakingly categorize sleep into stages (wake, REM, stage N1–N3) in 30-s epochs, the progression of which is called a hypnogram (B). The multitaper sleep EEG spectrogram (C) takes only seconds to estimate and reveals patterns of oscillatory dynamics that correspond closely to the rough architecture of the hypnogram. The spectrogram shows spectral power (color: cool \rightarrow warm:low \rightarrow high power) as a function of time (x-axis) and frequency (y-axis). Furthermore, the multitaper spectrogram provides a visually striking characterization of the continuum of brain oscillatory activity during sleep, providing information that is lost in a typical hypnogram. Additionally, the multitaper sleep spectrogram can describe an entire night of sleep in a single visualization, whereas the EEG waveform trace of the same data (D) provides no detailed information at this scale.

and Kleitman (4, 30). This paved the way for the Rechtschaffen and Kales (R&K) system in 1968 (77), which classified sleep into 30-s epochs of Wake, REM, and four stages of non-REM (NREM). The use of 30-s epochs is a procedural relic from the 1930s, when Loomis et al. used a paper tape system to physically plot the EEG, which automatically cut the paper into 30-cm strips with the paper moving at 1 cm/s. Almost 50 years later, R&K scoring is still the clinical standard for sleep medicine and sleep research, with minor adjustments such as reducing NREM to three stages (N1–N3) (42). As such, sleep staging based on R&K scoring has long served as a useful tool and an essential foundation for numerous important advances in sleep research and in clinical sleep medicine.

The use of sleep staging, however, comes with several substantial drawbacks. In practice, sleep staging is a time-consuming process, requiring highly trained sleep technicians to visually categorize hours of waveform data in hundreds of non-overlapping 30-s epochs. Sleep staging is also subjective, since the sleep stage within each epoch is determined by eye based on the technician's interpretation of the waveform data and application of the staging rules. Consequently, achieving consistency between scorers is an ongoing concern. Even for sleep in healthy subjects, the average rate of disagreement between experienced technicians is ~20%, and it can take several years for a technician to learn to score at this level of accuracy. In cases of pathological sleep, the inter-scorer variability increases even further, since the oscillatory activity does not fall neatly into the guidelines for one of the pre-defined sleep stages and thus cannot be adequately characterized by the hypnogram (36, 37, 83). Sleep staging is therefore also inflexible, in that a finite set of stage definitions is unlikely to support characterization of the vast heterogeneity in the sleep EEG observed in both healthy and clinical populations.

From a data analysis standpoint, sleep staging reduces the information-rich, dynamic, and continuous process of sleep to an abstract, low-resolution summary of discrete semantic states. Thus, no matter how sophisticated analysis techniques and scientific studies become, they will ultimately be limited if the results must always be referenced back to the framework of the hypnogram, which discretizes sleep in time and in state. Sleep staging discretizes sleep in time by defining the hypnogram in non-overlapping 30-s epochs, a length of time based on historical convention and practicality, rather than a principled analysis of sleep dynamics. By placing a temporal constraint upon the data, sleep staging imposes the assumption that

sleep state cannot change any faster than every 30 s and that the neural activity within each epoch is not changing. This assumption reduces the ability to characterize sleep states that are shorter than 30 s, such as sleep microstates. Consequently, the analysis of transient EEG phenomena is either performed manually—such as periodic limb movements of sleep (PLMS), cortical EEG arousals—or remains un-quantified in clinical work (e.g., spindles, K-complexes, cyclic alternating pattern). Objective characterization of these brief events may prove clinically important to complement the extensive work on the disruptions associated with obstructive sleep apnea (OSA) and, perhaps to a lesser degree, PLMS. Sleep staging also discretizes sleep in state by restricting sleep states to only five possibilities (i.e., Wake, REM, NREM stage 1–3), making it impossible to represent sleep phenomena that vary along a continuum. Overall, the resolution in visual sleep staging is limited to the qualitative features in the EEG that can be practically discerned and categorized by the human eye. Attempts to improve staging by defining a greater number of stages over smaller epochs (39, 80) have not been adopted in the field, in part because these enhanced resolution sleep-staging paradigms are even more laborious than the current standard. Given the need to analyze brief changes in the EEG and to characterize a continuum of neural states, it is therefore important to have an objective, quantitative analysis of the EEG that minimizes subjectivity and the need for discretization.

Perhaps most notably, the use of discrete sleep stages does not match our current understanding of sleep neurophysiological dynamics. In the half-century since R&K scoring was initially proposed, there have been enormous advances in our knowledge of the neural mechanisms of sleep. During this time, in effectively every dimension studied, sleep has been shown to be a continuous dynamic process (67) involving the activity of numerous cortical and subcortical networks that generate and coordinate neural activity at multiple frequencies (13). Additionally, with the recent advent of optogenetic (1) and pharmacogenetic (81) techniques in rodents, the specific cell types responsible for the state-dependent control of cortical oscillations are now being revealed in greater detail (21, 38, 47, 86). Studies have also shown that some aspects of neural activity during sleep may be locally regulated (52, 66, 97), a feature that cannot be captured by traditional sleep staging. In fact, individual cortical regions can exhibit features of sleep in an awake animal (97). The converse may occur in insomnia (51).

Given this growing body of mechanistic knowledge, it stands to reason that the neural oscillations observable in human EEG could act as a direct link to the activity of specific networks and cell types in-

volved in sleep. Furthermore, deviations in the sleep EEG could provide fundamental insights into the pathophysiology underlying sleep-related disorders. By representing sleep as a coarsely discretized progression of abstract stages, all of this potentially vital neurophysiological information is lost. Thus it is essential to strive toward a characterization of sleep EEG oscillations that faithfully represent the underlying data, allowing us to apply the wealth of knowledge we have gained about the continuum of the underlying neurophysiological mechanisms to the interpretation of the EEG.

Toward these ends, a powerful tool for analyzing sleep EEG oscillatory structure has been spectral analysis, a quantitative approach for describing a waveform signal in terms of its underlying oscillations (sinusoids) at different frequencies. The power spectrum is a function that represents the strength (power) of those oscillations at each frequency. Spectral analysis also encompasses analysis of time-varying oscillations using the spectrogram, which plots signal power as a function of time and frequency, making it possible to observe how the frequency structure changes over time (FIGURE 1C). Spectrograms are therefore well suited to characterize the temporal evolution of sleep-related neural oscillations at different frequencies over the course of a night of sleep.

While the benefits of spectral analysis were recognized by sleep researchers as early as the 1980s, embodied in variants of the spectrogram such as the color density spectral array (CDSA) (78, 79), density spectral array (DSA) (72), or hypnogram (49, 50), the impact of these early efforts was constrained in part by the technical limitations of spectral estimation procedures in common use during that time. Methods such as the periodogram provide inaccurate (biased) and noisy (variable) estimates of the power spectrum and spectrogram (75). Spectra estimated with these techniques can therefore be difficult to interpret, with noisy and ill-defined spectral peaks that may obscure important features of sleep EEG dynamics. The differences in spectrogram quality between common spectral estimation methods is illustrated in FIGURE 2.

One common method for improving poor EEG spectral estimates has been to average spectral power within canonical frequency bands. For example, sleep analyses may report the total power within delta (0.5–4 Hz), theta (4–8 Hz), alpha (8–12 Hz), sigma (12–15 Hz), beta (15–30 Hz), or gamma (>30 Hz) bands. While averaging across frequencies reduces the variability in power over time, it greatly reduces the frequency resolution of the spectral estimate, producing a low-resolution estimate that looks like a step function (FIGURE 2,

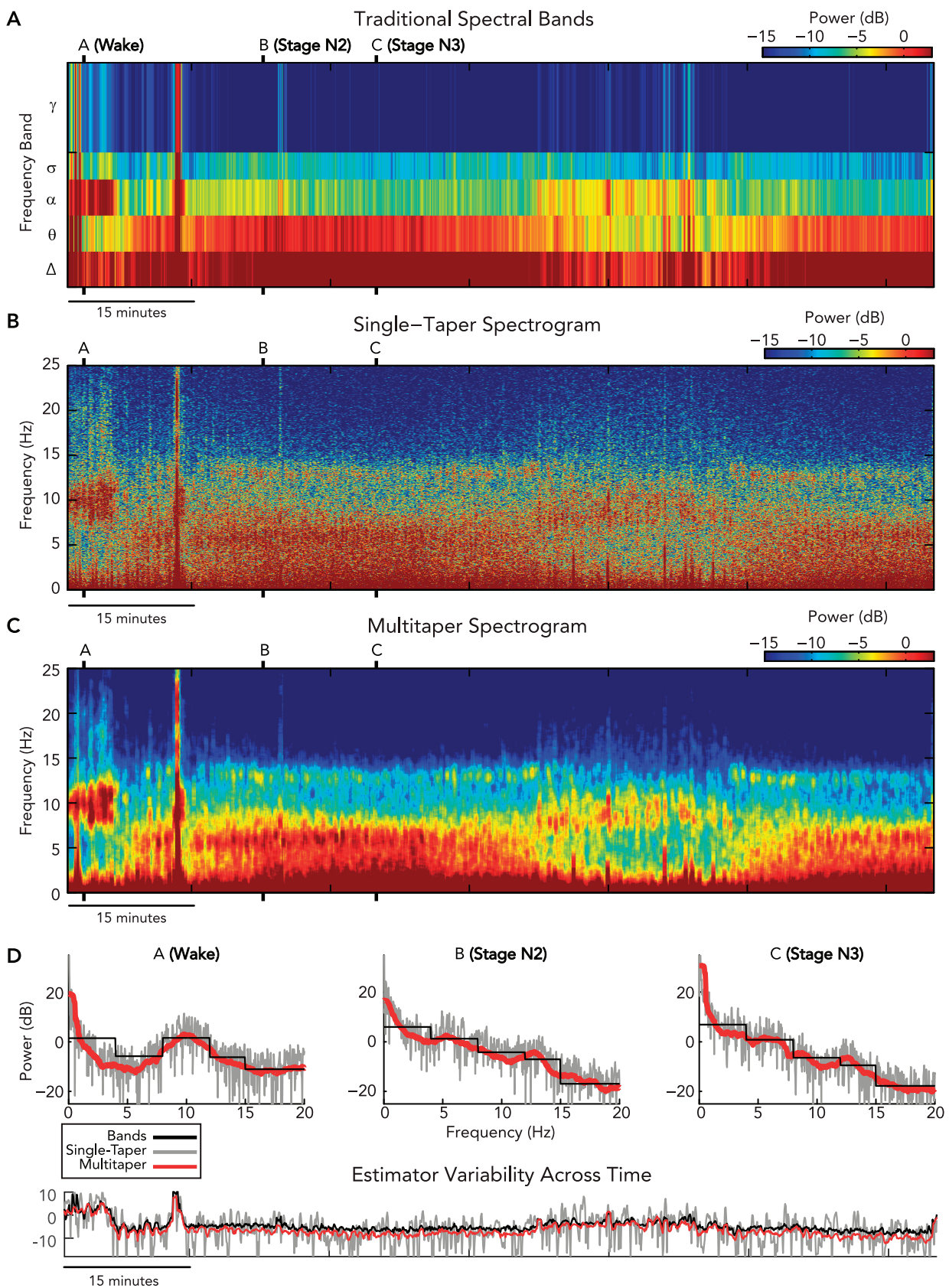
A AND D, black curves). In contrast, spectral estimation methods like the periodogram yield high-resolution spectra; however, the estimates are known to be inaccurate and noisy (FIGURE 2, B AND D, gray curves). A common approach to reducing variability in these estimates is to average these spectra across time, as in Welch's method (100), or as a function of state, such as sleep stage. While these time-averaging methods produce high-resolution, low-variance spectra, the temporal resolution is greatly reduced due to the additional smoothing across time. Thus it may appear that there is no middle ground in the trade-off between resolution (frequency or temporal) and variance. Fortunately, there exists a method called multitaper spectral estimation, which can produce clear, accurate, high-resolution spectral estimates, without having to average over frequency or time (FIGURE 2, C AND D, red curves).

In this paper, we review the neurophysiology of sleep through the lens of multitaper spectral analysis. We first present a primer of the basic theoretical and mathematical concepts underlying traditional spectral estimation and introduce the multitaper spectrogram (93) as a means of providing a high-resolution, low-noise, time-frequency representation of the sleep EEG. We will review the concepts of estimator bias and variance and explain how the multitaper method greatly improves on standard spectral analysis methods (12, 69). As we will demonstrate, application of the multitaper method makes clearly visible the relationships between spectral structure, traditional R&K scoring rules, and dynamics during a night of sleep that would be difficult to appreciate otherwise. We will then illustrate how the multitaper spectrogram can elegantly characterize the dynamics of the sleep EEG at full night (hours), ultradian (minutes), and microevent (seconds) time scales. We will detail the clear spectral motifs that comprise Wake, REM sleep, NREM sleep, and the transitions between them, and describe the connections between oscillatory features and the underlying neural mechanisms. Finally, we will discuss the clinical applications of the multitaper spectrogram using examples of clinical EEG data.

Through the course of reviewing the time-frequency representation of the sleep EEG, we will show that the multitaper spectrogram is an information-rich, multi-scale representation of the non-stationary spectral dynamics of the sleep EEG. By using the multitaper spectrogram to characterize the sleep EEG, we can make visible and quantify the continuous dynamics of multiple EEG oscillations in a way that the hypnogram cannot, while still making plain the features used in the construction of R&K sleep staging (FIGURE 1).

By reviewing sleep neurophysiology through this quantitative lens, we will show that principled time-frequency approaches can vividly characterize the activity and interaction of different

brain networks during sleep, providing a means to link the wealth of data acquired during polysomnography (PSG) with clinically important phenotypes and outcomes.



Methods

Theory and Methods of Spectral Estimation: Application to EEG Analysis

The goal of spectral estimation, sometimes called spectral density estimation, is to separate a waveform into different component oscillations based on frequency, just as a prism separates white light into a rainbow of different wavelengths or an equalizer in an audio system separates sound into different frequency bands. In general, spectral estimation takes any signal in the time domain (waveform traces as a function of time) and describes it in the frequency domain (spectral power as a function of frequency). The theoretical basis for spectral estimation is Fourier analysis (33, 46), which is a method that decomposes a time-domain signal into a series of pure sine waves of different wavelengths. This is particularly useful in the analysis of EEG data, where the signal represents the combined activity of multiple networks of neurons throughout the brain that oscillate at different frequencies.

A stationary periodic signal is one in which the frequency structure does not change over time. In stationary signals, it is appropriate to estimate a power spectrum, which represents the strength (spectral power) of the signal at different frequencies. **FIGURE 3A, TOP**, illustrates how multiple stationary oscillatory signals can sum into a single aggregate waveform with an intricate temporal structure. While the characteristics of the individual sinusoidal components are apparent when viewed separately, it is considerably more difficult to identify the number of underlying oscillations and their characteristics when viewing the aggregate waveform. By estimating the power spectrum of the signal, however, the number of oscillations, their frequencies, and their amplitudes become evident.

If the oscillatory structure of a signal changes over time, the signal is said to be time-varying or non-stationary. If the intention is to characterize how EEG oscillatory dynamics change in time, estimating a single power spectrum for the entire signal is not appropriate. Instead, a spectrogram may be estimated for time-varying signals. The spectrogram describes the power in the signal as a function of both frequency and time. This is some-

times referred to as looking at the data in the time-frequency domain. To represent data in the time-frequency domain, we can construct a spectrogram by estimating the power spectrum at different times using a moving window of data. The size of the data window is set such that the structure of the data within that window is approximately stationary. A spectrogram is visualized with the *x*-axis representing time, the *y*-axis representing frequency, and the spectral power represented by the color (cool → warm::low → high power) at each time-frequency point. **FIGURE 3B, TOP**, illustrates how multiple time-varying oscillatory signals sum into a single aggregate waveform. By computing the spectrogram (**FIGURE 3B, BOTTOM**), the temporal dynamics of the oscillatory structure become apparent.

In the analysis of EEG data, time-varying spectral analysis has numerous benefits. **FIGURE 3C, TOP**, shows an example of a typical EEG trace during the early stages of the sleep onset process. While the goal is to record only EEG data, it is common for other biological or external signals to “corrupt” a clinical recording. In this example, the raw signal contains the desired EEG data, but it also contains ECG activity as well as 60-Hz electrical noise. This makes the time-domain signal much harder to read, and thus it is much more difficult to characterize the underlying EEG activity. Consequently, this segment of data would likely be seen as corrupted and be thrown out, or filtering techniques might be applied to “clean up” the data. Simple band-pass filtering techniques are not necessarily an ideal solution, since they can distort the data and can prove inadequate in removing a complex signal. By using spectral analysis, however, no alteration of the data is necessary if the components of the waveform reside at different frequencies. In this case, the spectrogram (**FIGURE 3C, BOTTOM**) shows the electrical noise as a strong band at 60 Hz, and the ECG artifact as a band between 1 and 2 Hz. The EEG signal appears as an evolving band at 10 Hz, which in this example represents the eyes closed alpha oscillation of the subject starting to fall asleep.

Given the high suitability of time-varying spectral analysis for characterizing sleep EEG, why has it not yet taken hold in the field? Aside from overcoming the inertia associated with established procedures and the relative simplicity of classical

FIGURE 2. The multitaper method outperforms conventional spectral estimators, producing high-resolution EEG spectrograms with significantly reduced bias and variance

We estimated spectrograms from a single occipital EEG channel using periodogram-based frequency band averaging (A), single-taper Hanning window (B), and multitaper (C) approaches, each using 30-s windows spaced at 5-s intervals. In D, comparisons of spectra from each approach are shown using 30-s data windows from wake (marker A), NREM stage 2 (marker B), and NREM stage 3 (marker C) states. Below these spectra is a comparison of spectral power at 10 Hz for each method across time, illustrating differences in the temporal variability of each estimator. Traditional bands produce a low-resolution spectrogram (A) with coarse step-function spectra, but have low variability in power across time (D; black curves). Periodogram and single-taper spectrograms (B), while offering a high-frequency resolution, produce noisy spectra with ill-defined peaks and have a high temporal variability (D; gray curves). In contrast to these traditional approaches, the multitaper spectrogram (C) has a high-frequency resolution, shows clearly defined smooth oscillation peaks, and has low temporal variability (D; red curves).

sleep scoring, one reason may lie in the fact that the prevailing techniques for EEG spectral estimation produce noisy and inaccurate estimates of the power spectrum, making it difficult to interpret the resulting spectrogram. In this paper, we propose the use of multitaper spectral estimation, a method proven to greatly enhance the clarity of the spectral estimates over standard methods (12, 69). To appreciate the motivation for multitaper spectral estimation, it is important to understand the methods used in spectral estimation as well as the important considerations that must be made when performing spectral estimation on real data. We illustrate these considerations in FIGURE 4A using an example of a 10-Hz sinusoid.

Spectral estimation is based on Fourier analysis, an area of mathematics that provides a theoretical basis for breaking down a signal into its different frequency components. This theoretical analysis assumes that time-domain signals are infinite, continuous, periodic, and can be decomposed into pure sinusoids. Thus, given purely sinusoidal data of infinite length (FIGURE 4Aa), we can use Fourier analysis to estimate an ideal spectrum, which will be composed of perfect peaks (vertical lines) at each of the frequencies contained within the time domain signal (FIGURE 4Ab). These theoretical assumptions, however, break down when we analyze real data, which is finite, discrete, aperiodic, and

time-varying. Consequently, spectral analysis of real data can produce estimates that differ greatly from the ideal spectrum, producing inaccurate results and potentially leading to false conclusions. To obtain more meaningful spectral estimates for real data, we use different strategies to address the false theoretical assumptions, each of which comes with special considerations and tradeoffs. For example, EEG data are never truly stationary, so it is common to analyze small time segments of an experiment within which the data properties are assumed to be unchanging. While stationarity improves as the segments of data become smaller, our ability to discern oscillations at closely spaced frequencies decreases. The spectral resolution is defined as the smallest difference in frequencies that we can resolve. Thus there is a tradeoff between data window length and stationarity on one hand and spectral resolution on the other. In the following sections, we will describe the methods used for spectral estimation for EEG data and their pitfalls, followed by techniques for improving spectral accuracy (bias and resolution) and clarity (variance).

The Periodogram: “An Extremely Poor Spectral Estimator”

The simplest and most common method used for performing spectral estimation on EEG data is called the periodogram. In practice, the computation of the periodogram involves an algorithm

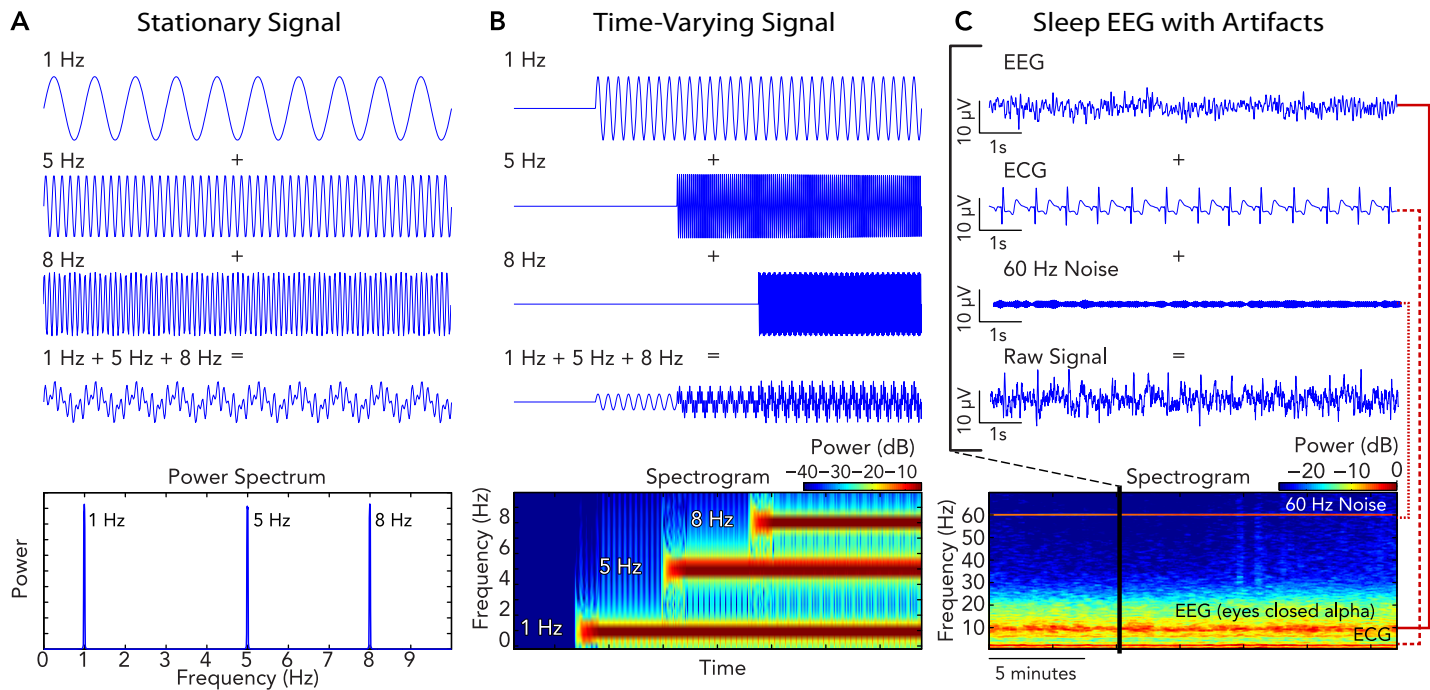


FIGURE 3. An overview of spectral estimation for stationary and time-varying signals

Spectral estimation using Fourier analysis assumes that any signal can be represented as the summation of multiple pure sine waves (A-C, top). For signals with stationary periodic structure (A), we can compute a single power spectrum (A, bottom), which represents strength of the signal at different frequencies. If the oscillatory structure of a signal is time-varying (B), we can compute a spectrogram (B, bottom) that tracks changes in the power spectrum over time. In practice, waveform EEG waveform data can be “corrupted” by other signals such as ECG and 60-Hz electrical noise (C, top), and may be discarded as an artifact. However, since these different signals occur at different frequencies, spectral analysis allows us to retain the data, viewing each signal independently in the time-frequency domain (C, bottom).

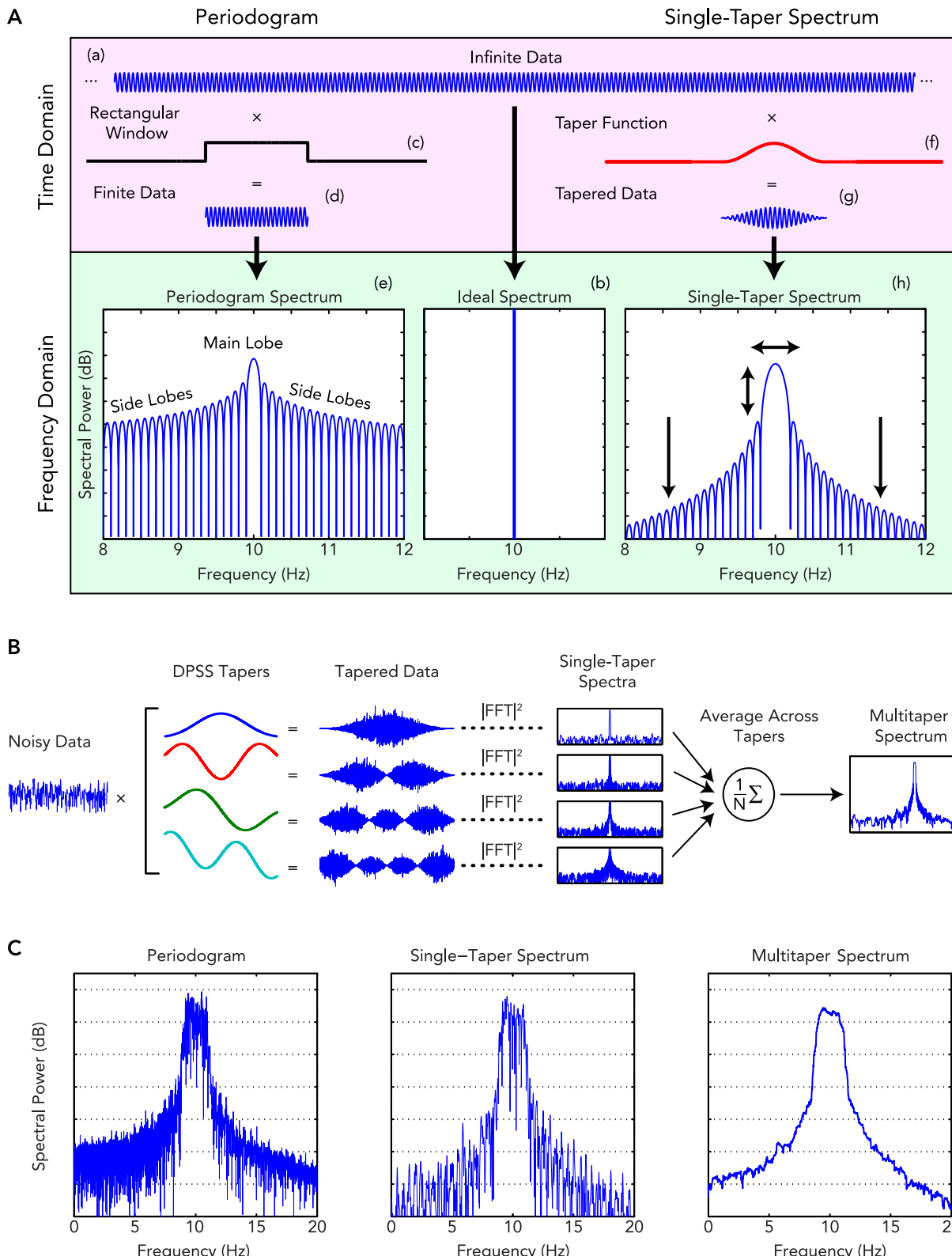


FIGURE 4. Multitaper spectral analysis reduces bias and variance in spectral estimation

A: An illustration of periodogram bias and the effects of tapering, using a 10-Hz sinusoid as an example. In theory, infinite data (a) yields a theoretical ideal spectrum with widthless peaks at each frequency (b). In practice, the periodogram of finite data (d) is an inaccurate (biased) and noisy (variable) spectral estimator (e), with a multi-peaked structure caused by sharp discontinuities imposed by finite data (c). Tapering reduces bias by taking the product of the data and a "taper" function (f) that smooths the discontinuities at the data ends (g). In doing so, tapering reduces bias by lowering the power in the side lobes of the spectrum (h).

B: A schematic of multitaper spectral estimation, which works by averaging multiple single-taper spectra that are computed using a special set of orthogonal functions.

C: A comparison of spectral estimates for a simulated noisy EEG spectral peak. The multitaper spectrum shows a smooth peak with greatly reduced noise compared with periodogram and single-taper (Hanning window) estimates.

called the fast Fourier transform (FFT), which is an efficient implementation of the Fourier transform for data in discrete time. Unfortunately, the periodogram has several suboptimal properties that cause major problems in spectral estimation. In fact, in his textbook *Spectral Analysis and Time Series* (75), Priestly calls the periodogram “ . . . an extremely poor (if not a useless) estimate of the spectral density function.” However, while rarely appearing in any state-of-the-art signal processing application, the periodogram (often incorrectly referred to as the “FFT”) is used widely and without reservation within the EEG literature.

What makes the periodogram such a poor estimator? When we compute the periodogram for a pure sinusoid in discrete time, instead of the single peak of the ideal spectrum, the periodogram estimate looks quite different. The resulting periodogram spectral estimate (**FIGURE 4Ae**) is comprised of a large rounded peak at the oscillation frequency, called the main lobe, flanked on both sides by a series of narrower peaks of decreasing power, called the side lobes. As we will soon see, the discrepancies between the periodogram and the ideal spectrum can cause major problems for EEG data analysis, and must be dealt with effectively to achieve accurate results.

Why does the periodogram spectrum differ from the ideal spectrum? An intuitive way of conceptualizing this phenomenon is to think of any finite data series (**FIGURE 4Ad**) as the product of infinite data (**FIGURE 4Aa**) and a rectangular or boxcar window (**FIGURE 4Ac**), with a value of 1 for the duration of the data and 0 everywhere else. Consequently, the periodogram of any finite data is the combination (convolution) of the ideal data spectrum with the spectrum of the rectangular window, which is a multipeaked function with a main lobe and side lobes. The periodogram of a single, finite sinusoid is the rectangular window spectrum centered at the main oscillation frequency. Generalized to all finite data, the periodogram will be the rectangular window spectrum replicated at each of the peaks in the ideal data spectrum, scaled by the amplitude of each peak (69).

How do these differences between the periodogram and the ideal spectrum affect the data analysis? The presence of side and main lobe power means that the periodogram of finite data is a biased estimator of the spectrum; that is, the estimated periodogram spectrum for real data will differ from the ideal (expected) spectrogram, especially in cases where the data length is small. The side and main lobes in the periodogram allow noise at a given frequency to “leak” into the estimate at other frequencies, distorting the true spectral content of the data. This spectral leakage, as it is called, reduces the accuracy of the estimate and

makes it more difficult to clearly distinguish peaks in the spectrum, especially in noisy data such as EEG.

The side and main lobes contribute to the periodogram bias in different ways. The side lobes introduce a broadband bias, which means noise across a broad range or band of frequencies is incorporated into the estimate. In our 10-Hz example, the ideal spectrum only has power at the central oscillation frequency. In contrast, the periodogram has side lobes that stretch out over all frequencies, falsely indicating the presence of broadband power. The power, which should be concentrated at a single frequency, is redistributed by the periodogram to frequencies where it does not belong. This broadband bias can be particularly problematic when data are noisy or have multiple closely spaced frequency peaks. In such cases, the side lobes in a periodogram act like transmitters, redistributing power from noise or multiple oscillations to unrelated frequencies. Thus, without taking measures to improve bias, an EEG periodogram can be easily corrupted by background noise, artifacts, and signals at frequencies unrelated to the oscillations being studied.

The main lobe of the periodogram is a source of narrowband bias, since it blurs all the frequencies within the small range of its bandwidth. This means that, if there are two oscillations that are separated by a frequency less than the width of the main lobe, they will be erroneously perceived as one oscillation. In the example of the 10-Hz sinusoid, the ideal peak has no width, yet the periodogram main lobe is a peak with an ~0.2-Hz bandwidth. The width of the main lobe therefore determines the spectral resolution of the estimated spectrum, which is the smallest difference in frequencies that can be distinguished by the spectral estimate. The spectral resolution also determines the smoothness of the estimate across frequencies—a coarser spectral resolution corresponds to a smoother spectral estimate, and vice versa. In practice, it is therefore important to select a spectral resolution that is less than the bandwidth of the oscillations that are to be analyzed in the data. We will later describe how to explicitly define the spectral resolution based on underlying assumptions about the oscillatory properties of the data.

The Single-Taper Spectrogram: Reducing Estimator Bias

Given the strong bias, the periodogram is an exceptionally inaccurate spectral estimation method. Fortunately, there are ways to greatly reduce periodogram bias. The most common method for improving periodogram bias is to apply a function called a taper or window function to the finite data before performing spectral estimation.

The result of this process can be called a single-taper spectrum. We recall that main and side lobes of the periodogram for finite data arise due to the sharp changes in the rectangular window at the start and end of the data. If we wish to reduce the bias caused by the side lobes, we must smooth out the abruptness of these transitions. By taking the product of the raw data and a taper function that has gradual transitions between 0 and 1 (FIGURE 4Af), the processed data (FIGURE 4Ag) becomes tapered at both ends (hence the name), decreasing the magnitude of the discontinuities. As a result, the power in the side lobes of the single-taper spectrum (FIGURE 4Ah) is greatly reduced compared with the periodogram (FIGURE 4Ae), and the difference in power between the main lobe and the highest of the side lobes is increased. This means that there will be less power from surrounding frequencies leaking into the spectral estimate, and thus the estimate will be less biased.

Another way to think about this process is that, by using a taper, the sharp rectangular window of the periodogram is effectively replaced by a smoother function with better spectral properties. In practice, many different types of functions can be used as tapers in computing the single-taper spectrogram. Typical tapers used include Hanning, Hamming, Blackman, Gaussian (often referred to as a Gabor transform), and Welch functions, each of which is designed to optimize different qualities of the spectrum for specific applications. When we use a Hanning window, a commonly used taper, in our 10-Hz example, the differences between the periodogram and single taper spectral estimates are clearly visible. Compared with the periodogram (FIGURE 4Ae), the power in the side lobes of the single-taper spectrum (FIGURE 4Ah) is greatly decreased, and the rate at which the power decreases at frequencies away from the peak is much greater. Additionally, the difference in power between the main lobe and the highest side lobes is increased. Consequently, the single-taper spectrum has far smaller total and relative contributions from off-peak frequencies, and thus will have significantly reduced broadband bias compared with the periodogram. Therefore, when the single-taper spectrogram is used with EEG data, we will be able to more accurately estimate oscillatory peaks than with a periodogram.

We also note that the width of the main lobe is slightly larger in the single-taper spectrogram than in the periodogram, which reduces the spectral resolution. In practice, there is a tradeoff between broadband (side lobe) and narrowband (main lobe) bias, which can be controlled by the choice of taper function. In any case, so long as the spectral

resolution is less than the bandwidth of the oscillations that are to be analyzed, the increase in the main lobe width should not cause any significant problems in the analysis.

The Multitaper Spectrum: Simultaneously Reducing Estimator Bias and Variance

Another major issue in spectral estimation is the concept of the variance of the spectral estimate, which characterizes the uncertainty in the estimate across frequencies. The periodogram produces estimates with high variance across all frequencies. This is illustrated in our example, where the ideal spectrum (FIGURE 4Ab) has a single vertical peak, whereas the periodogram has visible and highly variable side lobes (FIGURE 4Ae) around each peak. Thus the periodogram has a much higher variance than the ideal spectrogram. As the length of the data set length becomes larger, the variance of the periodogram remains constant. Thus, no matter how much data is collected, the periodogram estimate will not improve. Consequently, we call the periodogram an inconsistent estimator of the spectrum.

The variance of the spectral estimate is an especially important concern in EEG data analysis, requiring a high temporal resolution, which necessitates the use of relatively short data windows. Furthermore, while tapering reduces bias, it can actually increase the variance in short data sets. This is because tapering the data forces the time points near the ends to converge to zero (FIGURE 4Ag), effectively reducing the amount of data available to make the estimate and increasing the variance. Thus the analyses of short segments of noisy EEG data are prone to high variance, particularly when we use tapering to reduce the bias. How, then, can we produce a spectral estimate with low bias and a low variance for short segments of data?

In an ideal world, we could observe multiple independent measurements or trials of the same small time window of EEG activity. By averaging across all the single-taper spectra from each trial, we could cancel out the measurement noise and reduce the variance. However, given a single short segment of data, what can be done to reduce the variance? To address this problem, we can use a technique called multitaper spectral estimation (or the multitaper method), which was developed in the early 1980s by David Thomson (93) and has been shown to have superior statistical properties compared with single-taper spectral estimates (12, 69). The multitaper method works by averaging together multiple independent spectra estimated from a single segment of data. How is this possible? The innovation of the multitaper method is that, instead of using a single-taper function to compute

the spectrum, it uses multiple taper functions (hence the name) to compute single-taper spectra, which are averaged together. These tapers come from a particular class of functions called the discrete prolate spheroidal sequence (DPSS) (85). DPSS tapers are special because they are not only optimized to reduce bias, but they also have a special mathematical property called orthogonality, which enables them to extract uncorrelated single-taper spectral estimates from the same data. Because these single-taper estimates are uncorrelated with each other, they can be averaged together as if they were independent trials of the same condition, producing a spectrum with reduced variance. Another useful property of DPSS tapers is that they make it particularly easy to define the spectral frequency resolution and smoothness of the resulting spectrum.

Estimating the multitaper spectrum is therefore no more complicated than taking the average of several single-taper spectra. **FIGURE 4B** shows a schematic diagram for multitaper spectral estimation. Given a single segment of data, the steps for computing a multitaper spectrum are as follows.

Procedure 1: Multitaper Spectral Estimation

- 1) Generate a set of DPSS tapers given data assumptions (see *procedure 2*)
- 2) For each of the DPSS tapers, estimate a single-taper spectrum for the data
- 3) Compute the mean single-taper spectrum to form the multitaper spectral estimate

While this procedure is straightforward, it is important to understand the practical decisions that must be made when applying multitaper spectral estimation to real data, such as EEG, so that the analyses are principled and follow reasonable assumptions. In practice, multitaper spectral estimates are defined by several parameters, which control the number of DPSS tapers and their properties. These parameters are N , the size of the data segment in seconds; TW , the time-half-bandwidth product; and L , the number of tapers. By understanding these three parameters, it is possible to explicitly control features underlying the multitaper estimate. We outline a procedure, similar to that of Babadi and Brown (7), for choosing these parameter values.

To choose the values for these parameters, we must only know two things: the time period over which the data are thought to be stationary and the desired spectral resolution. First, the data segment size N should be defined as the maximum length of time (in seconds) at which the data are thought to be stationary. Practically, N should also reflect the scale of the dynamics that can be adequately observed at the time scale of the visualization. For

example, when looking at spectral dynamics across an entire night of sleep EEG data, we might choose N to be many tens of seconds long, whereas we would choose a much smaller N when performing an analysis of micro-arousals or spindles that occur on a time scale of seconds.

Next, the spectral resolution (Δf) is the bandwidth (in Hz) of the main lobe in the spectral estimate, which controls the minimum distance between peaks that we can resolve. In practice, a large Δf will produce smooth, low-resolution peaks, whereas a small Δf will produce higher-resolution peaks with greater detail. Typically, it is better to err on the side of a smaller Δf , so that potentially important spectral features are not overlooked.

Given these Δf and N , we can compute TW , the time-half-bandwidth product, as

$$TW = \frac{N\Delta f}{2} \quad (1)$$

where $TW \geq 1$. The time-half-bandwidth product (in Hz·s or dimensionless) is a parameter used in computing the DPSS tapers that relate the frequency resolution to the data window size, and is simply the product of the window duration (N) and half the bandwidth of the main lobe ($\Delta f/2$).

Finally, we must determine L , the number of tapers used in the estimate. Given TW , it has been shown that a choice of

$$L = \lfloor 2TW \rfloor - 1 \quad (2)$$

where the floor function $\lfloor \dots \rfloor$ rounds $2TW$ down to the closest integer, has desirable properties for efficient spectral estimation (7, 69). An expanded explanation of the rationale for this choice of L can be found in the APPENDIX.

The number of tapers is important, since it turns out that the variance of the spectral estimate is improved by a factor of L compared with a single-taper estimate. However, increasing the number of tapers means that the time-half-bandwidth product must be larger, which implies that the spectral resolution of the estimate will be reduced if N is fixed. It is thus important to account for the underlying assumptions about data stationarity and spectral resolution when adjusting L to minimize the variance.

For most applications, we suggest the following procedure for choosing the spectral estimation parameters.

Procedure 2: Selecting Multitaper Parameters

- 1) Set the window size N by determining the length of time over which the signal is thought to be stationary
- 2) Set the desired frequency resolution Δf , given the oscillatory structure of the data

- 3) Compute the time-half-bandwidth product as $TW = N\Delta f/2$
- 4) Compute the number of tapers as $L = 2TW - 1$

This procedure is simple to implement. For example, let us say that a signal is assumed to be stationary over 30-s intervals and that we desire a frequency resolution of 1 Hz. Given *Eq. 1*, it follows that $TW = N\Delta f/2 = (30 \text{ s} \times 1 \text{ Hz})/2 = 15$. We then plug the time-half-bandwidth product into *Eq. 2* and estimate the number of tapers as $L = \lfloor 2TW \rfloor - 1 = \lfloor 2 \times 15 \rfloor - 1 = 29$.

To compute the multitaper spectrogram, we estimate the multitaper spectra within temporal windows of size N , evenly spaced throughout the data record. It is common practice to overlap the windows by spacing them at intervals of $< N$. Overlapping does not change any of the stationarity assumptions of the spectral estimator; however, it provides a temporal interpolation of the data that may improve the ability to accurately resolve the timing of spectral events.

We now examine the effect of the multitaper procedure on the quality of the spectral estimate. **FIGURE 4C** shows the power spectrum of a short segment of simulated noisy EEG data with a 10-Hz broadband peak, akin to that of EEG alpha (8–12 Hz) power, as estimated by the periodogram (**FIGURE 4C, LEFT**), the Hanning single-taper spectrogram (**FIGURE 4C, MIDDLE**), and the multitaper spectrum (**FIGURE 4C, RIGHT**). The periodogram has a noisy peak that tapers off slowly, which indicates high bias and variance in the estimate. The single-taper Hanning spectrogram shows a reduction in bias, since the peak tapers down lower on each side compared with the periodogram. The variance of the single-taper estimate is slightly reduced from that of the periodogram, as evidenced by the smoother appearance of the peak. However, the magnitude of the noise within the spectral peak is increased as a result of the artificial shortening of the data caused by tapering. In contrast to the periodogram and single-taper estimates, the multitaper spectrum has a much clearer peak, reflecting a significant reduction in variance. Moreover, the bias of the multitaper estimate is similar to that of the single-taper estimate and is reduced compared with the periodogram. This falls in line with the finding (12) that, given control over bias, resolution, and variance, if two out of the three properties are held to be identical in multitaper vs. single-taper estimates, the third will always be superior in the multitaper estimate. In this case, the spectral resolution and degree of bias are fixed, and the multitaper estimate has greatly reduced variance compared with the single-taper estimate.

The theoretical improvements in spectral estimation bias and variance provided by the multita-

per method (7, 12, 69) are made even clearer when examining spectrograms for real EEG data. We return to the example in **FIGURE 2**, which shows the difference between spectrograms computed using traditional spectral bands (**FIGURE 2A**), a single-taper Hanning window (**FIGURE 2B**), and the multitaper method (**FIGURE 2C**) for a segment of a single channel of occipital EEG data during sleep. The single-taper spectrogram is very noisy due to the high estimator variance, and it is difficult to clearly distinguish oscillatory dynamics across time. In contrast, the multitaper spectrogram has a reduced variance, which reveals the dynamic interplay of neural oscillations. The reduction in variance is highlighted in **FIGURE 2C**, which shows the single-taper (gray) and multitaper (red) spectral estimates at time points corresponding to Wake (*marker A*), Stage N2 (*marker B*), and Stage N3 (*marker C*). In all cases, the single-taper estimates have high variability and a coarse structure compared with the multitaper estimates, which are smooth and have clearly defined spectral peaks.

Furthermore, the multitaper method can identify differences in the sleep EEG that are not possible to distinguish using traditional methods. To demonstrate this, we performed a statistical analysis showing that the reduced variance of the multitaper spectrogram can reveal differences in the sleep EEG that are too subtle to detect within the single-taper (Hanning) spectrogram. In particular, the multitaper spectrogram showed robust, statistically significant differences in EEG power across many frequencies when comparing late Stage N2 and early Stage N3, whereas the single-taper spectrogram found no clear significant frequency structure. An analysis of sleep during short transient peri-REM alpha bursts (16) yielded comparable results. These results strongly suggest that the low variance of the multitaper spectral estimate greatly facilitates the identification of sensitive features of neural activity and sleep architecture within the EEG. The details of the approach and results can be found in the APPENDIX and in **FIGURE 13**.

Other Basis Functions

Other basis functions have also been developed for spectral analysis. One common set of alternative basis functions are wavelets, which constitute a class of tapered, localized wave-like oscillations that can be easily scaled temporally. In fact, Fourier analysis can be considered to be a special case of wavelet analysis since sinusoids of different frequencies can be thought of as a single function that is temporally scaled. Wavelet decomposition (46, 60, 70, 71) is an excellent tool for spectral analysis and has high temporal specificity, a high sensitivity to low-amplitude signals, and a good time-frequency resolution tradeoff (94). Conse-

quently, wavelets are often used to analyze neural data. However, wavelets do not provide multiple independent estimates of the same underlying spectrum and therefore do not reduce the variance of spectral estimates in the way that multitaper estimation does. Thus wavelet estimates may be noisier and less statistically efficient than multitaper estimates. Additionally, wavelets are not optimized to reduce spectral leakage like DPSS tapers, so wavelet-based spectral estimates will have greater bias than multitaper estimates. Given that we are looking at networks of neurons with established oscillatory properties, frequency specificity is of the utmost importance in this particular domain. Thus using sinusoids with direct frequency representations rather than the "pseudo-frequencies" derived from non-sinusoidal wavelets makes a great deal of sense for neural data analysis. Moreover, given the vast amount of data in a single night of sleep and the ability of the multitaper spectrogram to characterize the EEG with a temporal resolution appropriate for established microevents, we believe that the temporal specificity of the multitaper method should be sufficient for this application. For a detailed theoretical and experimental comparison of multitaper and wavelet estimation for neural data, see Ref. 94.

In addition, other approaches, such as empirical mode decomposition (EMD), have been proposed as a means to estimate instantaneous frequency in rapidly time-varying signals (31a, 40a, 60a), such as event-related potentials and EEG microevents. However, the theoretical basis for these methods (40a), as well as their applicability to hours-long sleep EEG data with complex broadband structure, requires further study.

Data and Pre-Processing

Implementation. The multitaper spectrogram is constructed by estimating the multitaper spectrum in each of a set of data segments of fixed size, which can be overlapped for increased temporal continuity. By changing the parameters, spectrograms can be designed for clarity at different times scales. In this paper, we looked at the data on full-night, ultradian, and microevent time scales, choosing our parameters accordingly for each scale. For the full-night time scale, we focus on large-scale oscillation activity over many hours. We therefore chose parameters of $N = 30$ s spaced at 5-s intervals, $\Delta f = 1$ Hz, $TW = 15$, $L = 29$. For the ultradian spectrograms, we wanted to observe detail within the rapidly changing dynamics within a single sleep stage over the course of minutes. We therefore increased the temporal resolution while maintaining the same spectral resolution, choosing $N = 6$ s spaced at 0.25-s intervals, $\Delta f = 1$ Hz, $TW = 3$, $L = 5$. For the microevent spectrograms,

we wanted to observe short time dynamics occurring on a scale of only a few seconds. In this case, spectral resolution and estimate variance reduction are limited by the small window size needed to capture spindle and K-complex activity. We sacrificed frequency resolution to maintain a low-variance estimate within a small data window, choosing $N = 2.5$ s spaced at 0.05-s intervals, $\Delta f = 4$ Hz, $TW = 5$, $L = 9$ for our visualization.

The multitaper spectrograms were computed using the *mtspecgramc* function in the Chronux open source library (<http://www.chronux.org/>).

Experimental data and preprocessing. For the experimental data, 10 healthy right-handed subjects (5 women and 5 men) with ages ranging from 19 to 32 years (mean: 25.8 yr; SD: 5.09) and body mass index (BMI) of <30 slept for two consecutive nights in the Massachusetts General Hospital sleep laboratory. Subjects were prescreened to ensure a regular sleep schedule and no history of sleep disorder, psychiatric problem, or neurological disease, nor any history of tobacco or prescription/recreational drug use. We performed one night of home monitoring before the lab testing to exclude obstructive sleep apnea (OSA) [using a threshold of apnea-hypopnea index (AHI) < 5, and respiratory disturbance index (RDI) < 15] (WatchPAT, Itamar Medical). In addition, an experienced technician scored the experimental polysomnography (PSG) data following the first experimental night, and one subject was excluded after failing to meet the OSA criteria on the first night. Urine tests for drug use (Xalex Multi Drug Kit for 10 Drugs) were performed at screening and before each experimental night. Additionally, female subjects were screened for pregnancy. These studies were approved by the Human Research Committee Institutional Review Board (IRB) at the Massachusetts General Hospital.

Subjects were fit with a high-density (64-channel) EEG cap, as well as standard clinical polysomnogram sensors including pressure transducer airflow (PTAF), airflow, abdominal belt, and eye, chin, and limb electrodes. Visual staging of sleep data was performed before the statistical analysis by an experienced clinical sleep technician using contemporary American Academy of Sleep Medicine (AASM) guidelines (42).

The experimental data were processed using a 64-channel Brain Vision system with Laplacian referencing. The experimental spectrograms, excluding the single-channel examples, are the median spectrogram from the fronto-central or occipito-central eight-electrode montages, the details of which can be found in the APPENDIX.

Clinical data. De-identified clinical PSG data was selected from the Massachusetts General Hos-

Table 1. Summary of prominent oscillations and their proposed underlying mechanisms

Clinical Sleep EEG Oscillation Features			Proposed Mechanisms
Frequency Band	Frequency Range	Related Sleep States	Generating Networks/Regions and Neurotransmitters
Slow oscillation	<1 Hz	NREM	Cortically generated when excitatory brain stem cholinergic and aminergic influences are withdrawn. Up and down states involve periods of firing and silence of almost all cortical cell types, possibly initiated by deep-layer pyramidal neurons. Slow oscillations coordinate the timing of other NREM sleep rhythms (87, 90, 91).
K-complexes	<1.5 Hz	NREM	One cycle of the slow oscillation, coupled with a sleep spindle induced by cortical input to the TRN (22).
Delta	1–4 Hz	NREM	Complete withdrawal of excitatory aminergic and cholinergic inputs leads to a pronounced hyperpolarization of thalamocortical relay neurons initiating rhythmic activity due to an interplay of intrinsic membrane conductances (H-current, low-threshold calcium currents and calcium-activated potassium currents) (43, 44).
Theta	4–7 Hz	REM	Neocortical theta rhythms are not prominent during REM in humans. In rodents, prominent REM theta rhythms are due to rhythmic firing of pacemaker GABAergic neurons in the medial septum and entrainment of interneurons in hippocampus and related temporal lobe structures (96). In humans, theta bursts occur in the hippocampus during REM but are phasic not tonic, and the frequency is lower (20). Unclear whether mechanisms are similar to those described in rodents.
		NREM	Similar to alpha rhythms but with a lower level of activation of mGluR1a or muscarinic M3 receptors (41).
Alpha	8–12 Hz	Drowsy/Wake	Moderate activation of metabotropic glutamate receptors (cortical input) and/or muscarinic M3 receptors (brain stem input) leads to rhythmic high-threshold bursts in a subset of glutamatergic visual thalamic neurons that depolarize occipital cortical neurons and excite local interneurons resulting in phasic inhibition of thalamocortical relay neurons (41, 57, 58).
Sigma (spindles)	12–15 Hz	NREM REM NREM	Partial withdrawal of excitatory brain stem aminergic inputs leads to repetitive burst firing of GABAergic thalamic reticular nucleus (TRN) neurons. TRN bursting, in turn, causes hyperpolarization of glutamatergic thalamocortical neurons leading to a rebound burst in thalamocortical neurons and rhythmic depolarizations of cortical pyramidal neurons (5, 89).

pital Sleep Lab clinical database. These analyses were approved by the Human Research Committee (IRB) at the Massachusetts General Hospital. The clinical data were recorded using a standard PSG montage with contralateral mastoid referencing. Offline scoring by experienced technologists was performed according to AASM standards. Clinical spectrograms were computed from the median of the two occipital EEG channels, the details of which can be found in the APPENDIX.

Results

The multitaper spectrogram provides a clear representation of the spectral dynamics of the sleep EEG occurring at time scales ranging from seconds to multiple hours. In this section, we present representative examples of the high-density sleep EEG obtained in the sleep laboratory from young, healthy subjects at the full night, ultradian, and microevent

time scales. We then use this ideal data to describe the most common progression of spectral dynamics observed throughout sleep and link the oscillations observed in the multitaper spectrogram with their associated underlying neural mechanisms. A summary of the prominent oscillations involved in sleep and their proposed underlying mechanisms can be found in Table 1. In this way, we hope to outline a framework for describing neural activity during sleep in terms of oscillatory dynamics and network activity, which can provide a neurophysiologically principled platform for subsequent experimental and clinical analyses. While this is by no means an exhaustive atlas of the sleep oscillations and their topographical variations, this work illustrates the rich information potential residing in a single spectrogram and forms a framework of normative data, which can serve as a baseline for subsequent analyses of different clinical populations. We subsequently explore how this same

approach may be applied to low-density EEG within clinical settings.

The Full Night Sleep Spectrogram

One of the primary benefits of using the multitaper spectrogram is the ability to observe EEG dynamics across an entire night in a single visualization. In particular, we look at a visualization of median occipital activity, since all of the major sleep-related oscillations are visible in this region of the brain. While the features required to visually score EEG time traces become effectively unreadable at a time scale of only a few minutes, the spectral dynamics of the sleep EEG can be clearly observed over a time scale of many hours. **FIGURE 5** shows the occipital multitaper spectrogram of the sleep EEG of three different subjects (**FIGURE 5, BOTTOM**), along with the visual-scored hypnogram (**FIGURE 5, TOP**). Even without knowledge of the sleep EEG, it is possible to discern repeating multi-oscillation spectral motifs in the dynamic structure of the full night multitaper spectrogram that correspond well with the different aspects captured by the hypnogram architecture. Moreover, it is possible to discern differences in sleep architecture and oscillation structure between subjects.

Spectral Dynamics at the Ultradian Scale

At the coarsest level, sleep is segmented into periods of Wake, REM, and NREM, the constituent components of the ultradian cycle. Current clinical practice defines Wake and REM as unitary states, and NREM is divided into three discrete stages. The multitaper spectrogram makes plain the continuum of changes within and between each of these states. In the process of doing so, we will show that the EEG components used in traditional scoring also are represented in the time-frequency domain.

The Spectral Dynamics of Wakefulness and the Start of the Sleep Onset Process

The most conspicuous spectral feature of the EEG during the transition from wakefulness to sleep is high power in the alpha band (8–12 Hz) in EEG leads overlying the occipital cortex, as originally shown by Berger and Adrian (2, 3, 9) at the beginning of the 20th Century. As we show here, this alpha activity is high at the moment when eyes close, gradually decreases during the subsequent minutes, and abruptly dissipates at sleep onset. Thus inspection of the spectrogram can give an objective characterization of the sleep onset process. Occipital alpha waves are generated by the visual cortex and thalamus (11). Similar 10-Hz oscillations are also observed in the somatosensory cortex, where they are referred to as mu rhythms (45), and in the auditory cortex (53), where they are

referred to as tau rhythms. These alpha and alpha-like waves are thought to represent an idling state that occurs when sensory cortices are disengaged or inhibited (45, 48). Accordingly, alpha oscillations are reduced in size during sensory stimulation (45, 48, 53). Alpha waves can be modulated by attention, for instance, increasing in power in the visual cortex when visual information is “tuned out” (11, 64, 68).

Alpha rhythms appear to be governed in part by a unique class of thalamocortical neurons that synchronize via gap junctions and that burst preferentially at alpha frequencies when hyperpolarized (40). Recent animal studies suggest that a moderate level of cortical input, activating metabotropic glutamate receptor subtype 1a (41) or brain stem cholinergic input activating muscarinic receptor subtype M3 (57), leads to rhythmic burst firing at alpha-band frequencies in a subset of neurons in the visual thalamus (lateral geniculate nucleus) mediated by T-type calcium channels. These glutamatergic thalamocortical neurons rhythmically excite local GABAergic interneurons, which periodically silence tonically firing relay thalamocortical neurons (41, 57, 58). Two groups of thalamocortical neurons are suppressed at the positive or negative peak of the alpha rhythm, resulting in a dipole within visual cortex. Intrinsic burst firing of cortical pyramidal neurons at alpha frequencies may also contribute to the generation of the rhythm (84). Theta-band oscillations occurring in early NREM sleep are likely generated by similar mechanisms but with a lower level of cortical and/or brain stem input, resulting in a slowing of the intrinsic oscillation of thalamic neurons (41).

The act of falling asleep is a continuous, dynamic, multifocal neural process, with behavioral and physiological changes occurring with different dynamics throughout the period of sleep onset (67, 73). As mentioned, the most prominent hallmark of the sleep onset process is the appearance of a strong occipital oscillation in the alpha (8–12 Hz) band upon the closing of eyes during wakefulness, which is present in 90% of adults (**FIGURE 6**). As a subject falls asleep, the occipital alpha power gradually decreases, then becomes intermittent, and then disappears. The loss of alpha, which signifies scored Stage N1 sleep, is followed, after some interval, by a rise in power in delta (1–4 Hz) and theta (4–8 Hz), marking the start of NREM-related neural activity. Should the subject be aroused or wake up, the process rapidly reverses, with high power in delta and theta bands giving way to increased power in the alpha band, consistent with a re-instatement of brain stem cholinergic inputs. Recent studies have shown that the latency between thalamic and cortical deactivation during the loss of alpha and rise of low-frequency oscilla-

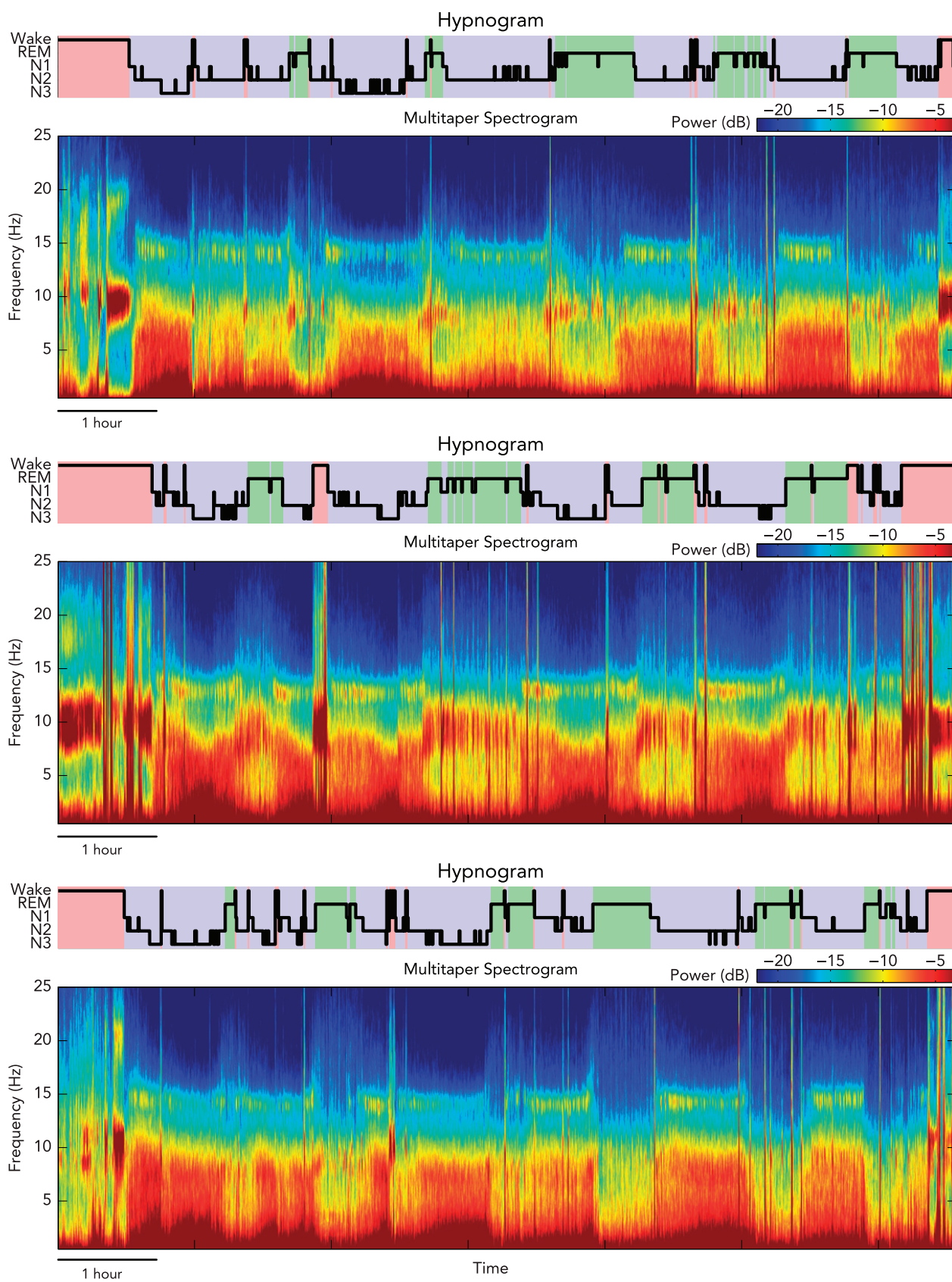


FIGURE 5. The multitaper sleep EEG spectrogram can clearly characterize the sleep oscillation architecture of a full night in a single visualization

The technician-scored clinical hypnogram (top), and multitaper occipital sleep EEG spectrograms (bottom) are presented for three different subjects. In each case, the spectral dynamics within multitaper spectrograms correspond well with the hypnogram while also revealing the continuous oscillatory dynamics associated with the activity of specific cortical and subcortical networks during sleep.

tions is highly variable (59) and that some subjects can exhibit a delay of several minutes between the loss of alpha before the low-frequency rise, during which time behavior continues as if the subjects were awake (73). These results suggest that it is therefore the presence of low-frequency power that inhibits behavior during sleep onset rather than the loss of alpha.

The EEG spectral dynamics of wakefulness and the sleep onset period are illustrated in **FIGURE 6A**, which shows the occipital multitaper spectrogram from a subject during the start of the sleep onset period. Initially, when the subject is quiescent with open eyes, the spectrogram has low power across all frequencies. When the subject's eyes close, the spectrogram changes dramatically, showing strong spectral power with a central frequency at ~9 Hz. In general, this oscillation falls within the range of 8–12

Hz, which is called the alpha band. Due to the imperfect sinusoidal structure of the alpha oscillation, it is also common to observe spectral power at the second alpha harmonic, which is two times the central frequency of the alpha oscillation. In this case, the alpha harmonic appears at ~18 Hz. As the sleep onset process progresses, the oscillation power and bandwidth in alpha gradually decrease, then fluctuate, then disappear. The disappearance of alpha aligns well with the start of technician scored Stage N1. With the loss of power in alpha, the spectrogram shows a broadband increase in low-frequency power, in particular in frequencies spanning the slow/delta (0.5–4 Hz) and theta (4–8 Hz) bands. The sudden subsequent disappearance of the power in delta/theta and reemergence of power in alpha signifies an arousal to wakefulness, which also aligns well with the hypnogram. The spectrogram then

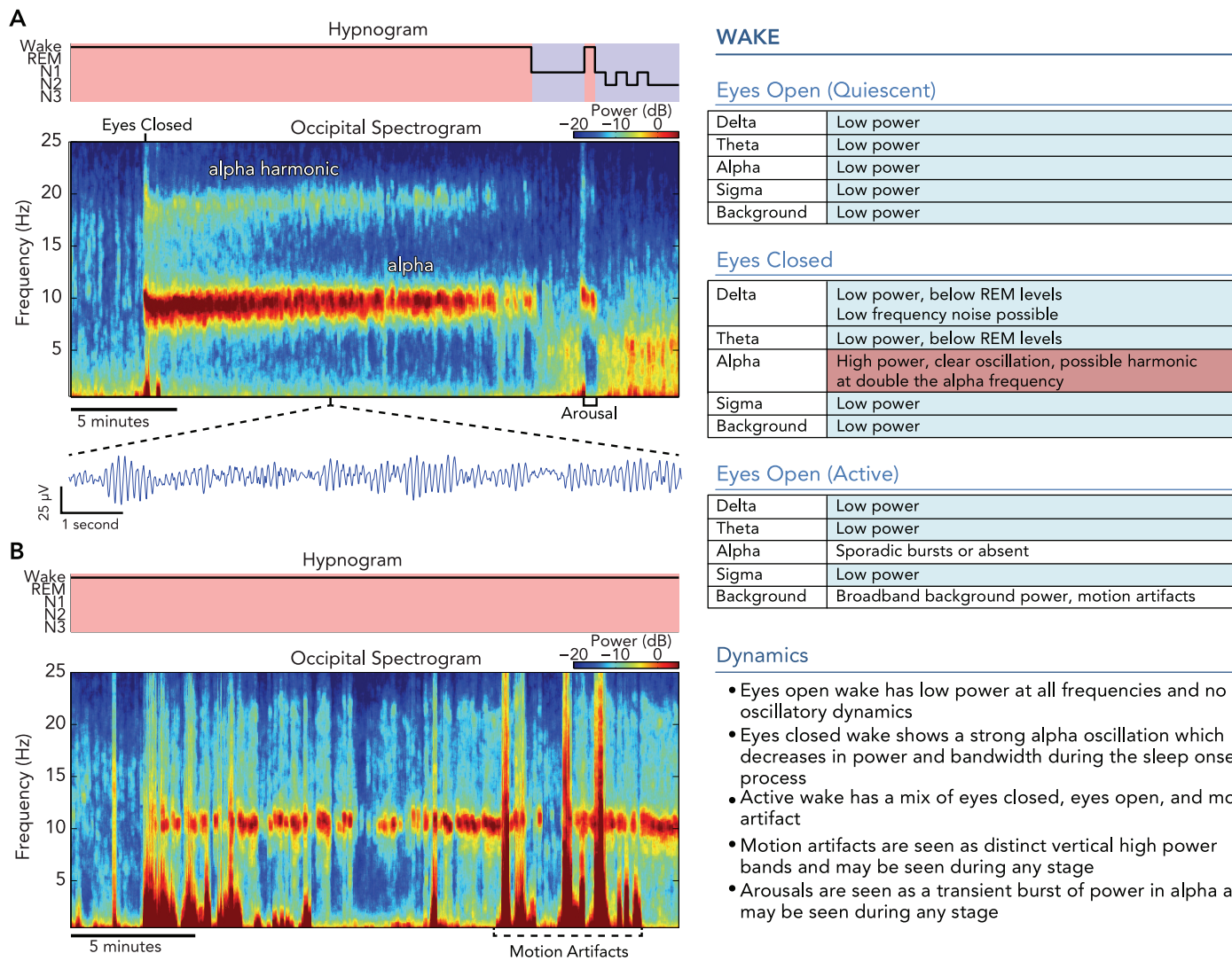


FIGURE 6. The multitaper characterization of EEG spectral dynamics associated with quiescent sleep onset and active wakefulness

During quiescent wakefulness as a subject falls asleep (A), a strong occipital oscillation in the alpha band appears when the eyes are closed, then gradually decreases before dropping out at the initiation of NREM sleep. Arousals throughout sleep are indicated by strong, transient alpha power. Active wakefulness (B) is associated with a variety of spectral patterns corresponding to different physiological states, including motion artifacts, which appear as strong broadband power. Motion artifacts are also hallmarks of arousals accompanied by motion during the night.

shows a reversal back to a high-delta-/theta state without power in alpha, indicating that the subject has fallen back to sleep. Thus, using the multitaper spectrogram, it is possible to characterize the sleep onset dynamics of this subject with a single visualization.

It is also useful to be able to identify nonquiescent wakefulness common at the early stages of a sleep study or experiment. **FIGURE 6B** shows the occipital multitaper spectrogram for a different subject during a restless period of waking drowsiness. Overall, these periods show a mix of eyes open wakefulness and transient alpha with broadband background noise. Additionally, strong subject movement appears in the spectrogram as vertical lines spanning all frequencies. While these motion artifacts are not part of the EEG signal, they provide important information regarding the quiescence of the subject (or lack thereof) during wakefulness. Motion artifacts are also important during sleep, since they accompany arousals that can appear throughout the night (see **FIGURE 6A** at the moment of arousal).

The Spectral Dynamics of the NREM Continuum

Clinically, NREM sleep is divided into three stages (Stages N1–N3) using thresholds on the amount of delta and theta oscillations as well as spindles and K-complexes observed within a given 30-s epoch of sleep EEG based on visual inspection (42). While these guidelines provide simple rules by which to categorize degrees of NREM sleep by eye, a great deal of information is lost by limiting the progression of NREM to only three possible states, between which the transitions are instantaneous. In contrast, the multitaper spectrogram reveals the information-rich continuum of spectral dynamics of NREM sleep, providing a robust visual and quantitative framework for understanding the activity, interactions, and neural mechanisms of the underlying oscillations.

The most striking spectral feature of Stage N2 sleep is the presence of increased power in the sigma band (12–15 Hz). On closer inspection, both in time domain and in higher time resolution spectrograms, this increased sigma band power occurs in transient ~1-s bursts that are referred to as sleep spindles (**FIGURES 7 AND 8**). Sleep spindles are thalamocortical oscillations that are initiated by rhythmic bursts of action potentials in GABAergic neurons in the thalamic reticular nucleus (TRN), whose burst firing is mediated by Cav3.3 T-type calcium channels (6). These bursts of action potentials lead to large inhibitory postsynaptic potentials in thalamic relay neurons. This hyperpolarization removes the inactivation of a different subtype of T-type calcium channels (Cav3.1), resulting in a

shorter, stereotyped burst of action potentials in relay neurons. The burst of action potentials in glutamatergic relay neurons leads to a depolarization of cortical pyramidal neurons (reflected in the EEG recording) and a reactivation of TRN neurons, completing the cycle (5, 89). Interconnections of TRN neurons via electrical and chemical synapses control the level of synchronization of the bursting within functionally coupled groups of TRN neurons. The extent of this synchronization determines the power and duration of the spindle recorded in the EEG. The spindle frequency itself is determined primarily by the kinetics of the synaptic potentials in the thalamic relay and TRN neurons, in particular the decay of the IPSPs in relay neurons. Recent human studies suggest that spindles are not uniform but differ in frequency and cortical topography, reflecting activity in different thalamocortical circuits (29, 66). Clinical studies have identified prominent abnormalities in sleep spindles in schizophrenia (61–63) and other severe disorders such as autism (55) and mental retardation (82), and correlated these abnormalities to deficits in sleep-dependent memory consolidation (98). Recent studies comparing manual, automated, and crowd-sourced scoring methods have underscored the fact that scoring of these clinically relevant events manually is an imprecise and time-consuming task (99), and is not performed in clinical analysis. As we show here (**FIGURES 7 AND 8**), the multitaper spectrogram provides a useful way to characterize spindles and ascertain their frequency.

Stage N3 sleep is characterized by increased low-frequency EEG power in the slow-oscillation (<1 Hz) and delta (1–4 Hz) bands, occurring in at least 20% of an epoch. Slow oscillations reflect local synchronous periods of inactivity in cortical neurons that are likely influenced by thalamic connections (25, 66, 87, 88, 90, 91). These periods of neuronal inactivity are often referred to as “down” or “off” states (22, 66). Delta (1–4 Hz) rhythms are thought to be generated primarily by the thalamus through the interaction of intrinsic voltage-dependent conductances of thalamocortical neurons (43, 44). Withdrawal of excitatory brain stem cholinergic and aminergic influences on relay neurons abolishes the tonic firing of these neurons observed during wakefulness and causes them to hyperpolarize, placing them in a rhythmic mode of firing where bursts are generated at a delta frequency (40). This hyperpolarization brings the membrane potential to a range where hyperpolarization-activated cation channels (encoded by HCN genes) can open, leading to a so-called H current as well as de-inactivation of low-threshold calcium channels. The H current provides a depolarizing drive, which returns the membrane poten-

tial to threshold, leading to a low-threshold calcium spike and a burst of action potentials. The after-hyperpolarization caused by the influx of calcium during this burst and subsequent activation of calcium-activated potassium channels cause a hyperpolarization that restarts the cycle. During this phase of sleep, TRN neurons are more hyperpolarized, preventing the occurrence of spindle oscillations. The frequency range of this activity and its highly synchronized nature, along with other biochemical evidence and computational considerations, led Tononi and Cirelli (24) to propose that such slow-wave activity serves to

depress or depotentiate the majority of excitatory cortical synapses, providing a homeostatic mechanism to prevent saturation of synaptic efficacy. Although not universally accepted, this theory provides one potential mechanism by which sleep may benefit learning. Slow oscillations are also associated with opening of the brain's glial-mediated lymphatic system, or "glymphatic" system, which permits clearance of beta amyloid proteins that are implicated in the development of Alzheimer's disease (102). As can be easily seen in the multitaper spectrogram, such slow and delta-band activity is high and

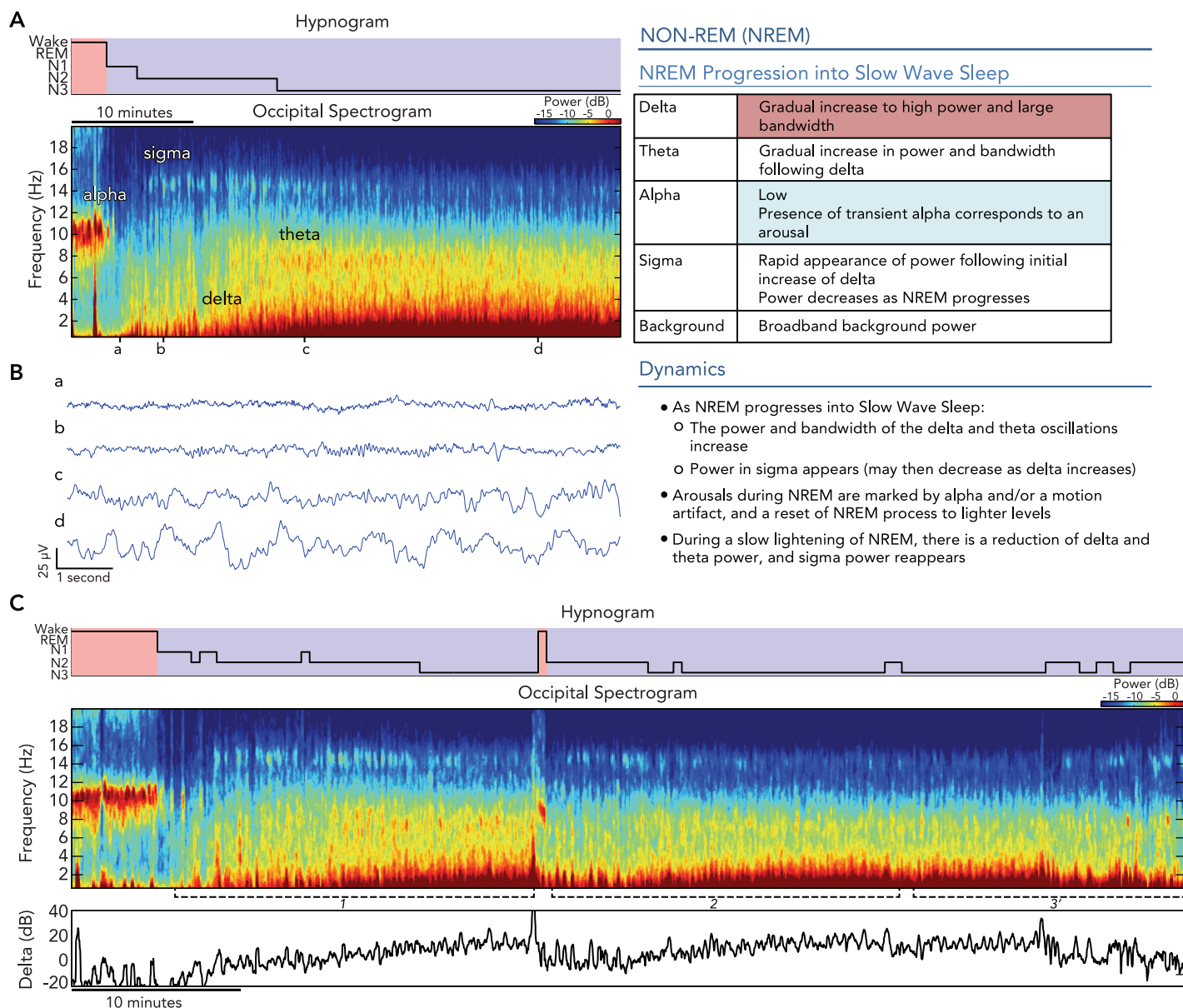


FIGURE 7. The multitaper characterization of EEG spectral dynamics associated with sleep onset and the continuous NREM progression into slow-wave sleep.

During the sleep-onset process, oscillation power in alpha gives way to a continuous progression into slow-wave sleep, with increasing delta and theta power and a rise and fall of sigma power. This gradual transition is clearly visible in the multitaper occipital spectrogram (A), as well as in the time domain traces (B). The transition into slow-wave sleep forms a spectral motif that is repeated after an arousal (C, markers 1 and 2). This progression can be reversed during the lightening of NREM sleep (C, marker 3), with a gradual reduction in delta and theta power, as well as a return of sigma power.

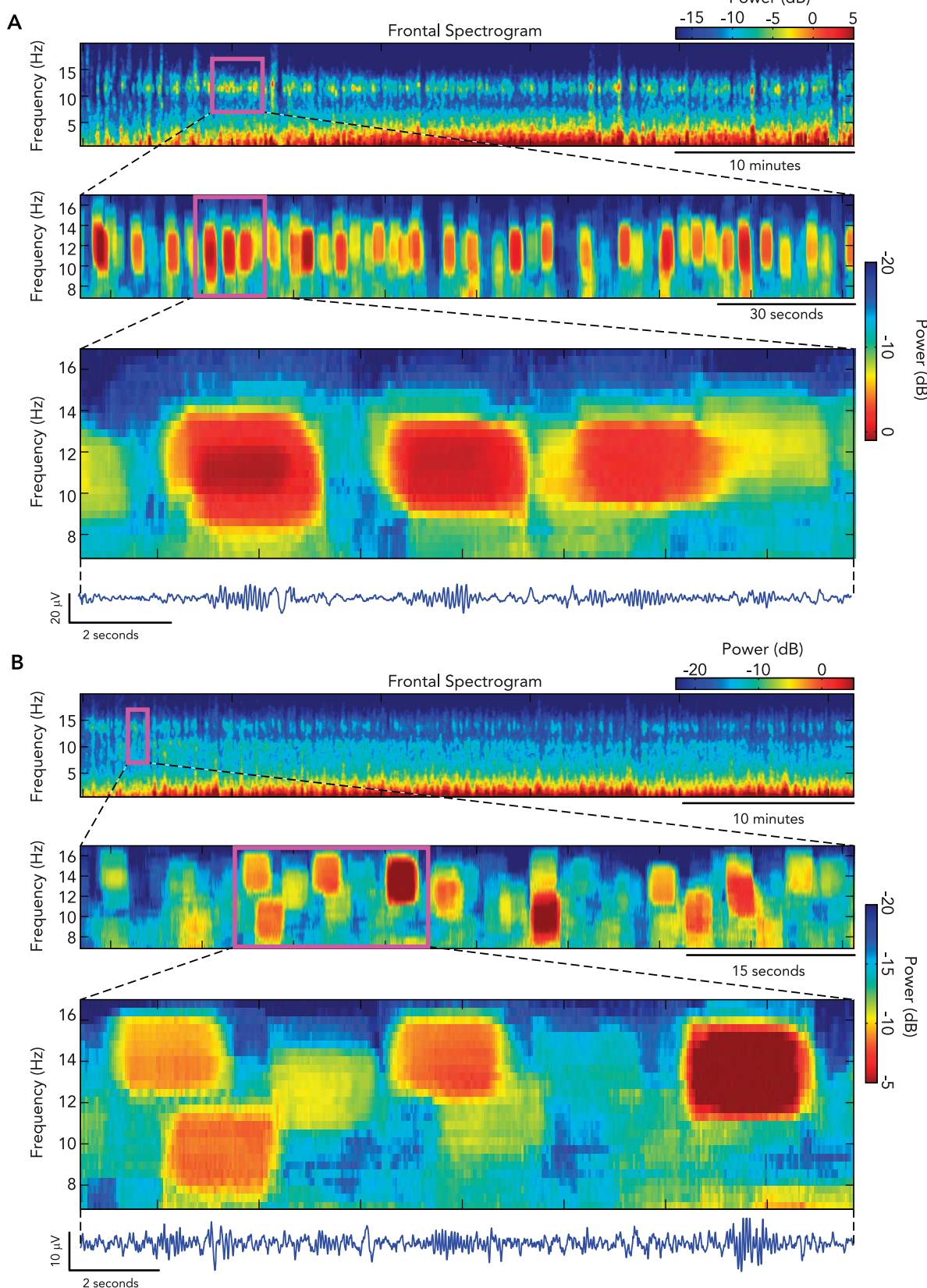


FIGURE 8. The multitaper spectrogram clearly represents spindles as distinct regions of transient spectral power

A multi-scale visualization of the frontal EEG spectrogram shows spindles centered around a single frequency (A) in one subject, and "high" and "low" spindles in another subject (B). By using the multitaper spectrogram, it can be much easier to disambiguate distinct overlapping spindles at different frequencies than in the time-domain traces (bottom).

consolidated early during the night but becomes more fragmented and less intense later in the night when REM sleep becomes more prominent. Conversely, in many sleep disorders and other neurological conditions, sleep is more fragmented and less slow-wave activity is observed, possibly accounting in part for diminished daytime cognitive performance. Classic sleep scoring is less useful to fully assess this fragmentation since the relatively long 30-s epochs do not allow the assessment of brief events.

FIGURE 7A shows the occipital multitaper sleep spectrogram from a subject during the progression from scored Wake to Stage N1, N2, and N3. During this progression, we observe the continuous dynamics of oscillations in alpha, delta, sigma, and theta, as well as the equivalent time-domain traces (**FIGURE 7B**). Initially, just as in **FIGURE 6A**, the subject goes through the sleep onset process, in which strong power in alpha (note the motion artifact) transitions to broadband low-frequency power at the start of scored Stage N1. This broadband oscillation has a sharp peak near 1 Hz and grows continuously in both amplitude and bandwidth during the progression of NREM sleep. Shortly after the onset of the low broadband power, the spindle-related oscillation in sigma appears, corresponding with the scored Stage N2. As NREM progresses, power in sigma gradually decreases in both amplitude and bandwidth. Around the time of scored Stage N3, a spectral peak in theta power appears, which also decreases in power and bandwidth as NREM continues.

Although delta and theta power are traditionally viewed as two separate entities, it is important to consider the source of the oscillatory power. During the NREM progression, we see a low-frequency oscillation with a long-tailed bandwidth that increases into the theta range. In addition, we see a distinct oscillation with a clearly resolved peak that falls within the theta range. In the case of the low-frequency oscillation, power in theta will be directly linked to the low-frequency (delta) power since it is merely the tail of the same oscillation. In contrast, the activity in a distinct theta oscillation may be uncorrelated and be generated by completely different networks than the low-frequency oscillation. Similarly, at the beginning of sleep, theta activity may simply reflect a slow alpha oscillation (41). By using the multitaper spectrogram, we can easily distinguish between a distinct oscillation residing within a specific frequency range and broadband power that happens to span that frequency range.

Overall, **FIGURE 7A** illustrates the principal spectral motif of NREM sleep, variations of which can

be seen repeated throughout the night. We can therefore use this knowledge to characterize larger scale NREM dynamics and sleep fragmentation. **FIGURE 7C** shows the occipital multitaper spectrogram from a different subject during a disrupted bout of NREM. In this example, the NREM spectral motif is repeated three times, aligning well with both the hypnogram (**FIGURE 7C, TOP**) and total observed delta power dynamics (**FIGURE 7C, BOTTOM**). The first motif appears during the sleep onset process, in which eyes-closed alpha transitions to the oscillations of NREM sleep (**FIGURE 7C, repetition 1**). As the power in sigma and theta starts to decline, the subject has an arousal to wakefulness, marked by a motion artifact followed by a short burst of power in alpha. The oscillation in delta immediately resets to low power and small bandwidth, and then the NREM process starts again for the second time (**FIGURE 7C, repetition 2**). A subsequent reduction in delta oscillation power and bandwidth indicates a lightening of NREM sleep, often linked to a scored arousal. If there is progressive lightening of sleep, we will see the same spectral dynamics of NREM motif but in reverse. In this case, the subject lightens (**FIGURE 7C, repetition 3'**) and power in delta gradually decreases, while power in theta and sigma starts to appear again.

Thus, by understanding the progression of oscillation dynamics during a single, uninterrupted bout of NREM, it becomes straightforward to characterize the general course and fragmentation of NREM throughout the entire night of sleep.

NREM Microevent Spectral Dynamics

Spindles. Clinical sleep scoring rules define sleep spindles as 11- to 16-Hz frontal-central oscillations lasting 0.5 s or more (42). The broadness of this definition and the difficulty of visually gauging the precise oscillation frequency in the time domain make scoring of spindles time-consuming and variable (99). Moreover, there is cross-subject heterogeneity in spindle morphology (10, 27, 28, 31, 101), which makes the creation of a one-size-fits-all automated classifier challenging (76). The multitaper spectrogram, however, provides a clear picture of the putative spindles that comprise transient sigma band activity.

FIGURE 8 shows examples of the frontal multitaper spectrogram of two different subjects during NREM. The sigma band appears to be a cohesive oscillation when viewed at a time scale of tens of minutes (**FIGURE 8, TOP**) or more. However, when examining the data on a time scale of a few minutes, it becomes clear that the sigma band power is comprised of many spindles, which appear in the

spectrogram as well defined transient peaks of spectral power (FIGURE 8, MIDDLE). On a time scale of a few seconds, the central frequency and duration of the spindle spectral peaks can be readily discerned and align well with time domain (FIGURE 8, BOTTOM).

While traditional time domain spindle scoring is the most straightforward in subjects with clear consistent spindles (FIGURE 8A), it is much more difficult to visually discern spindles in subjects in which the morphology is highly variable or with the superposition of “fast” and “slow” spindles (FIGURE 8B). In contrast, the multitaper spectrogram representation can be easily interpreted regardless of the variability in spectral morphology, since the frequency decomposition provides a clear separation between spectral peaks of different frequencies.

K-complexes. K-complexes are transient low-frequency oscillations that reflect brief periods of

reduced cortical neuronal activity, or so-called “down” states (22). K-complexes occur spontaneously during NREM sleep but may also be elicited by sensory stimuli (22). In the multitaper spectrogram, K-complexes appear as brief periods of broadband power in low frequencies. FIGURE 9 shows the occipital multitaper spectrogram of K-complexes during NREM, aligned with the time domain trace. K-complexes may be readily distinguished from motion artifacts, as the spectral power quickly attenuates by 2–3 Hz, and the duration is shorter. FIGURE 9 shows examples of the multitaper spectrogram of K-complexes in reference to the NREM progression.

The Spectral Dynamics Surrounding REM Sleep

REM sleep is defined by an “activated” EEG and a loss of muscle tone (4, 30). In rodent and cat studies, theta-band activity dominates the EEG during

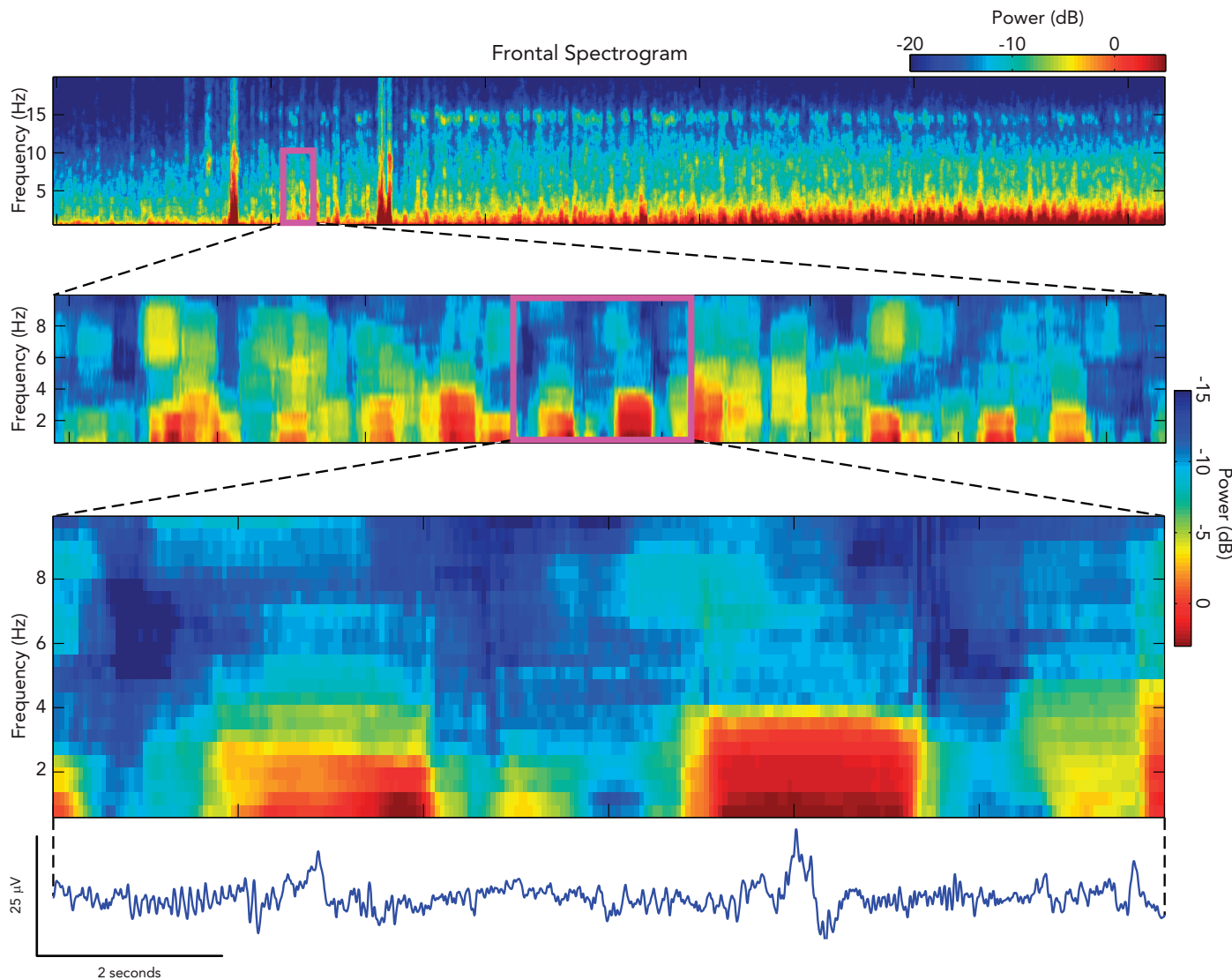
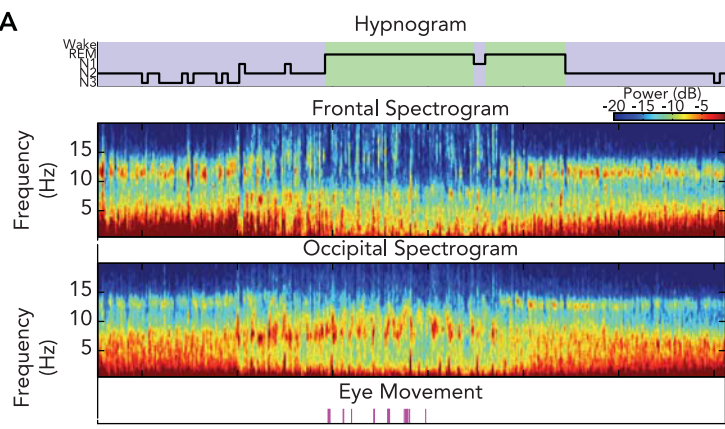


FIGURE 9. The multitaper spectrogram represents K-complex activity as transient low-frequency power

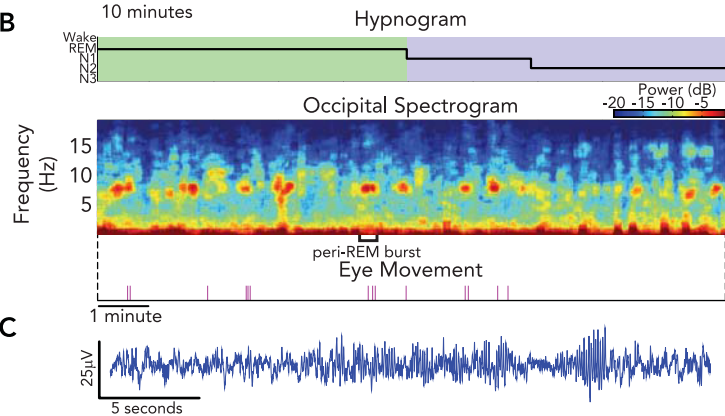
A multi-scale visualization of the spectrogram into the frontal EEG spectrogram shows the spectral signatures of K-complexes during the start of NREM.

A**THE REM PERIOD**

Delta	Rapid decrease to low power following NREM
Theta	Rapid decrease to low power following NREM
Alpha	Recurring transient occipital power in low-alpha frequencies
Sigma	Low power
Background	Background power level above that observed during Eyes Closed Wake

Dynamics

- From NREM, delta and theta power and bandwidth rapidly decrease
- From NREM, sigma power disappears
- Background power is higher than during eyes-closed Wake

B**Peri-REM Alpha Bursting**

- Subjects can exhibit transient, recurring bursts occipitally in low-alpha frequencies
- The bursts:
 - Have lower power, bandwidth, and peak frequency than the alpha seen during eyes-closed Wake
 - Begin to appear at the end of the preceding NREM period and may continue into the next NREM period
 - Decrease in temporal recurrence as REM progresses
 - Burst frequency changes across the peri-REM period

C

FIGURE 10. The multitaper characterization of EEG spectral dynamics associated with the REM sleep and transitional periods
During the initiation of REM sleep, low-frequency power drops off, and background power increases. Additionally, transient occipital alpha bursting can be observed in NREM preceding and following the scored REM period. In A, the multitaper spectrogram shows the EEG spectral dynamics in the surrounding 1-h period of scored REM, with peri-REM alpha bursting visible in the occipital spectrogram. Eye movement occurs sporadically throughout scored REM. In a second subject, a shorter time scale (12 min) reveals the clear transient alpha power of the peri-REM bursts, which can continue many minutes after rapid eye movements have stopped. The time-domain waveform of a single peri-REM burst (B; bracket region) is shown in C.

this state due largely to the dorsal location of the hippocampal formation and the prominent role in theta rhythms in rodent behavior (96). In humans, theta activity is more phasic (20) and of lower frequency. In mice and children, theta activity has been observed in the EEG just before bouts of cataplexy, a condition in which REM atonia is triggered during wakefulness by emotional arousal (95). This suggests that the theta activity observed during REM sleep could be linked mechanistically to REM atonia. In clinical sleep scoring, REM is scored as a single, monolithic state, but REM has been separated out into at least two parts: a tonic REM and a phasic REM consisting of muscle twitches and rapid eye movements. Although not observed in the clinical EEG, in animal studies (26) or deep brain recordings in humans (32, 54), ponto-geniculo-occipital waves, events which are likely involved in dreaming, can also be observed. Multitaper spectrograms of the EEG and electromyogram (EMG) are ideal for distinguishing tonic and phasic activity and the dissociation of EEG and EMG activity that occur during symptoms of narcolepsy such as sleep paralysis, as well as impaired

muscle atonia in REM sleep behavior disorder due to degeneration of caudally projecting neurons in the subcoeruleus (SubC)/sublateral dorsal (SLD) nuclei of the dorsal pons (13, 34).

In R&K scoring, the EEG of REM sleep is defined as having a low-amplitude signal comprised of mixed frequencies, sawtooth waves, and the absence of spindles or K-complexes (42). While not an explicit component of the scoring criteria, power in alpha is also commonly observed, especially in younger subjects. In practice, REM sleep is most easily defined through the presence of rapid eye movements, as well as low power with transient bursts of muscle activity in the EMG. While this assortment of multi-modal observations comprising REM sleep suggests a plurality of evolving processes, REM is scored as a single state into which the subject instantly transitions. In contrast, as we show in FIGURE 10A, the multitaper EEG spectrogram shows a gradual progression of oscillatory changes spanning traditionally defined REM. FIGURE 10A shows 60 min of the frontal (FIGURE 10A, TOP) and occipital (FIGURE 10A, MIDDLE) multitaper spectrum from a different subject transition-

ing from NREM to REM then back to NREM. While the hypnogram depicts a series of instantaneous transitions, the multitaper spectrogram shows gradual changes in the EEG activity during this period. Before the scored REM period, we observe a gradual transition out of NREM, with a decrease in low-frequency power and a decrease in sigma power. Similarly, we see the reverse sequence of spectral events, an increase in slow and sigma power, before the end of scored REM.

Peri-REM Low-Alpha Bursting

The multitaper spectrogram provides a computational basis with which to visualize the oscillatory structure of the sleep EEG on a larger time scale than the time domain, which makes it possible to observe phenomena not readily apparent in 30-s epochs. FIGURE 10A shows the period surrounding a bout of scored REM for another subject, but on a time scale of ~10 min. During the transition out of NREM, the occipital spectrogram shows transient increases in occipital power in low-alpha frequencies, which may persist through scored REM into the next bout of NREM. Plotting the times of rapid eye movements against the spectrogram (FIGURE 10B, BOTTOM) shows that certain REM alpha bursts may be correlated with shifts between tonic and phasic REM. We refer to these transient alpha oscillations during REM as peri-REM low-alpha bursts, or simply peri-REM alpha bursts.

While transient alpha power during REM has been studied in great detail by Cantero (15–19), this obvious feature of REM sleep microstructure is absent in R&K scoring. This is perhaps because individual bursts may not be long enough to trigger a scored arousal or epoch of Wake and would be too time consuming to score manually. By using the multitaper spectrogram, these peri-REM alpha bursts can be easily identified and can be used as not only an indicator of REM but also as a powerful predictor of impending REM onset during NREM.

Spectral Motifs Within the Context of a Full-Night Spectrogram

Given the spectral motifs observed around scored Wake, NREM, and peri-REM epochs, it is possible to quickly characterize the sleep EEG from the full-night occipital multitaper spectrogram. Take, for example, the multitaper spectrogram in FIGURE 1C. We first see the signatures of nonquiescent wakefulness (FIGURE 6B), followed by waking power in alpha (FIGURE 6A). We see the sleep onset process, in which power in alpha transitions to the NREM spectral motif (FIGURE 7A) at ~1 h (1:00) into the record. By examining the changes in power and bandwidth in delta and theta, along with the corresponding changes in sigma, the dynamics of the

fragmentation in NREM can be readily discerned (FIGURE 7B). After deepening, lightening, and deepening in NREM again (~1:00–3:00), the EEG transitions into the peri-REM spectral motif (~3:00–3:30), with the periodic peaks in alpha and reduced low-frequency power (FIGURE 10A). Note that the low-frequency power is visibly higher than that during eyes-closed alpha and that the power in alpha itself is persistent during wakefulness and thus appears more vividly in the spectrogram. The EEG then successively transitions between NREM and peri-REM motifs four more times (~3:30–9:30), with a period of wakeful power in alpha in the last of the NREM bouts (~8:30). Through examining the changes in spectral power during each of these NREM periods, it is possible to describe the differences in duration of fragmentation at a more precise level if required. The final motif of NREM activity changes to an eyes-closed alpha followed by a mixed period of quiescent and nonquiescent wakefulness as the subject wakes up (~9:30–10:30). Throughout the record, motion artifacts can be seen as faint vertical lines, providing insight into arousals and lightening of NREM sleep.

Characterizing Other Signals: Muscle Activity

The multitaper spectrogram can also characterize other biosignals such as muscle activity. FIGURE 11 shows examples of chin EMG multitaper spectrogram (FIGURE 11, TOP, with corresponding time-domain traces) (FIGURE 11, BOTTOM) for periods surrounding scored Wake (FIGURE 11A) and REM (FIGURE 11B) sleep. Wakefulness is characterized by prolonged periods of high muscle tone, represented by persistent broadband power in the spectrogram, the power of which falls away during sleep onset. Transient low-powered muscle twitching is common during REM sleep, which is visible in short broadband bursts in the EMG spectrogram. Analysis of EMG could be helpful in quickly disambiguating periods such as REM and Stage N1, in which EEG activity is similar but EMG activity differs.

Applications to Clinical Analysis

In the preceding sections, we have used high-density EEG under experimental conditions to demonstrate the ability of the multitaper spectrogram to provide a clear characterization of neurophysiological oscillations during sleep on multiple time scales. Given the ease of this characterization, the multitaper spectrogram has great potential as a tool to supplement standard clinical analysis and to offer greater diagnostic efficiency. As an illustration of the feasibility of this approach under clinical conditions, we analyzed the six-channel clinical EEG data from patients

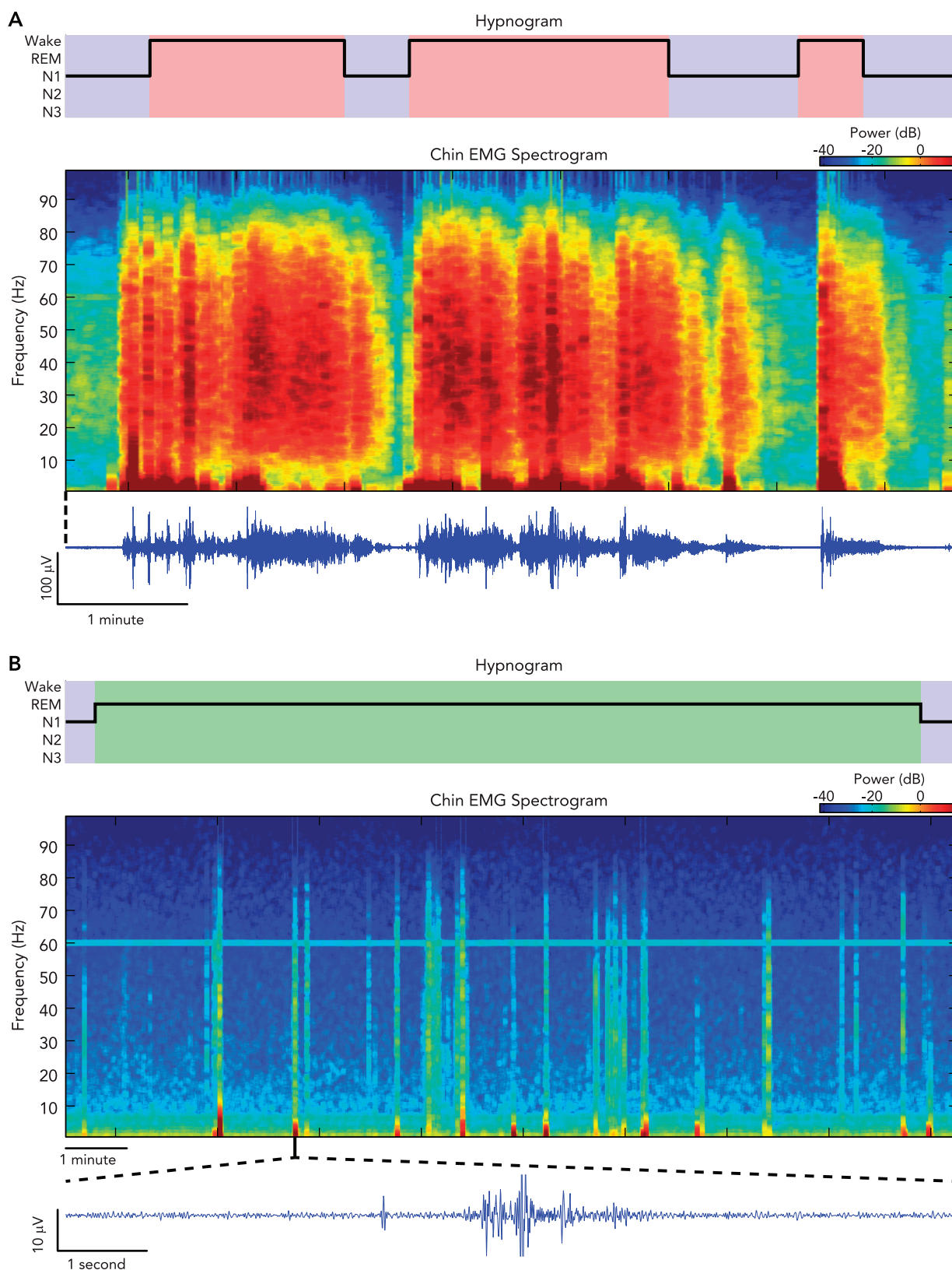


FIGURE 11. The multitaper spectrogram can also characterize other biosignals such as muscle activity. The chin EMG multitaper spectrogram (top) and time-domain trace (bottom) are shown for time periods surrounding scored Wake (A) and REM (B) epochs. Muscle activity during wakefulness has prolonged periods of high muscle tone, represented by persistent broadband power in the spectrogram, the power of which falls away during sleep onset. Transient low-powered muscle twitching is common during REM sleep, which is visible in short broadband bursts in the EMG spectrogram.

undergoing PSG testing at the Massachusetts General Hospital Sleep Laboratory.

Multitaper Sleep Spectrogram Characterization of Disrupted Sleep

As an example of potential clinical utility, we use the multitaper sleep EEG spectrogram to illustrate fragmentation of NREM during respiratory events like sleep apnea. In **FIGURE 12A**, the hypnogram (**FIGURE 12, TOP**), occipital clinical multitaper sleep EEG spectrogram (**FIGURE 12A, MIDDLE**), and the timing of technician-scored respiratory events (**FIGURE 12A, BOTTOM**) are shown for a subject with obstructive sleep apnea (OSA) (AHI: 27.9). The multitaper spectrogram reveals a dramatic change during a series of respiratory events (apnea and hypopnea) occurring during a NREM sleep. At the onset of the respiratory events, the low-frequency power typical of NREM becomes fragmented, with suppression of low-frequency power that coincides with bursts of power in delta/theta, alpha, and sigma at each respiratory event. While this fragmentation of EEG activity and resulting “arousals” have been observed in the time-domain traces, the multitaper spectrum allows us to more easily view the correspondence between apnea events and the EEG on a much larger time scale. The ability to observe and characterize these events and relationships could provide a means of rapidly identifying the occurrence and context of apnea events, and could replace the current clinical practice of painstakingly identifying individual events in the time-domain.

Sleep Staging from Multitaper Spectrograms

In the preceding sections, we have shown that all of the features used in R&K scoring are visible in the multitaper spectrogram. It follows that the multitaper sleep spectrogram could provide a means to rapidly characterize sleep architecture in clinical settings. As proof-of-concept of this hypothesis, one of the authors (M.P.) scored 16 clinical sleep records: 8 from patients without any sleep disorders and 8 from patients with either moderate-severe OSA or elevated periodic limb movements of sleep (PLMS). Visual staging of each record into Wake, NREM, and REM epochs was performed using clinical EEG multitaper spectrograms alone, with the scorer blind to the time-domain traces, any other PSG signals (eye movement, EMG, respiration, etc.), and any information about the clinical condition of the patient. Transitions between stages could be marked at any point of time. Scoring was performed using custom software that allowed for annotation of full-night and ultradian level multitaper spectrograms (as detailed in this paper) for each of the six clinical EEG channels, as well as the mean of the two occipital leads (see **FIGURE 14** in the APPENDIX). This spectral scoring

was then compared with the clinical sleep R&K stages scored by technicians using the full PSG.

The results of this proof-of-concept experiment showed that there was no significant difference between the epochs of Wake, REM, and NREM scored by technicians using R&K scoring and the full PSG and epochs scored using only the sleep EEG multitaper spectrograms (Cohen's Kappa = 0.71, $P < .0001$ given H_0 : categorical agreements occurred by chance). To examine the clinical applicability of these results, we compared the apnea-hypopnea index (AHI) and respiratory disturbance index (RDI), two clinical indexes used for measuring the severity of sleep apnea, using tech-scored and spectrogram-scored estimates of total sleep time (TST), the denominator in these calculations. While spectral scoring tended to estimate a shorter TST than tech scoring (median difference: 21 min), there was no significant difference between the clinical designations derived from the two methods. For both AHI and RDI, 15 of the 16 records (93%) fell within the same clinical category for apnea severity (normal, mild, moderate, severe), with a Cohen's Kappa of 0.86 and 0.83 for AHI and RDI, respectively ($P < .0001$ given H_0 : categorical agreements occurred by chance). Moreover, spectrogram-based scoring required on average only 5.2 min for each record (range: 1.6–10.0 min; SD: 2.7 min). Overall, these results suggest that the multitaper spectrogram is an efficient tool for characterizing sleep that can produce clinically equivalent diagnostic results based on TST, in addition to providing rich information not captured by the traditional staging hypnogram.

Discussion

In this work, we have rigorously detailed the advantageous statistical properties of multitaper spectral estimation over the periodogram and single-taper spectral estimates, and have illustrated the application of the multitaper spectrogram to the analysis of sleep EEG spectral dynamics. Furthermore, we have provided strong statistical evidence that multitaper spectral analysis can identify differences in the sleep EEG that cannot be distinguished using traditional single-taper methods (see APPENDIX). We have contrasted and compared the multitaper spectrogram to traditional sleep scoring, and demonstrated proof-of-concept for different domains of clinical application. Overall, the multitaper spectrogram provides a precise characterization of the continuum of complex oscillatory dynamics in the brain during sleep and wakefulness, and contains a wealth of information lost in traditional sleep scoring. Thus the multitaper spectrogram enables a rich empirical frame-

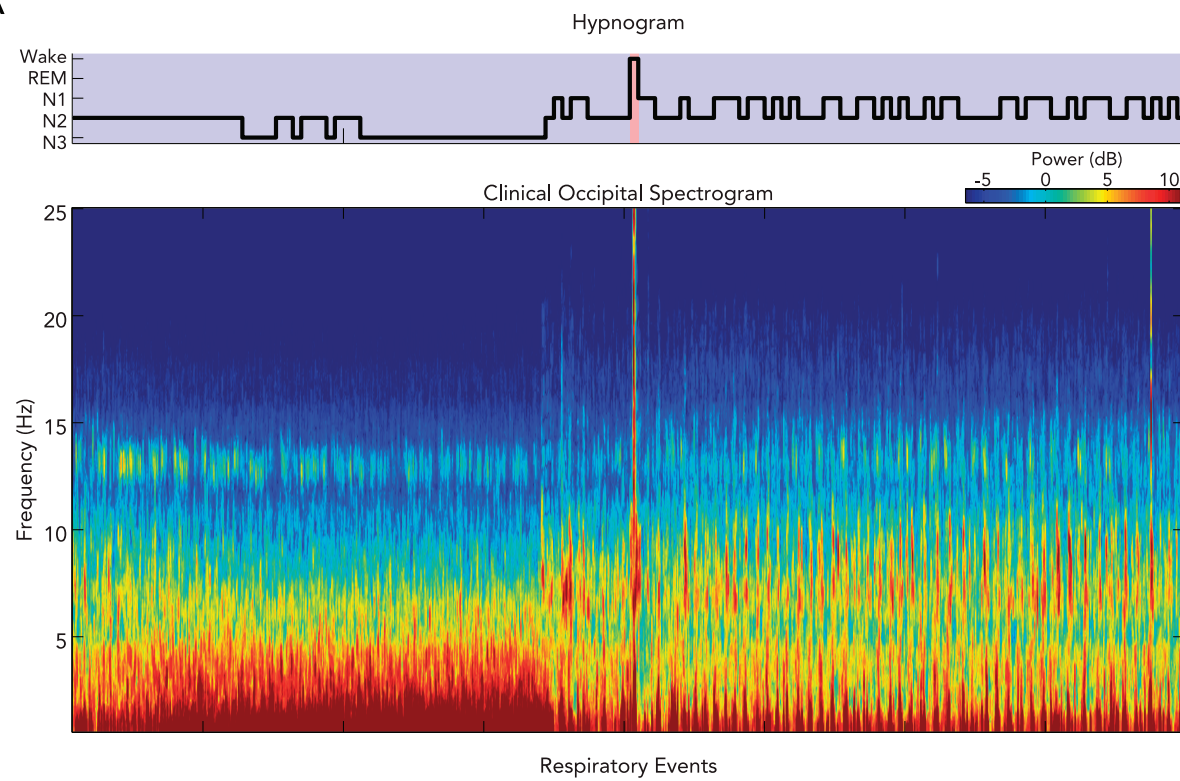
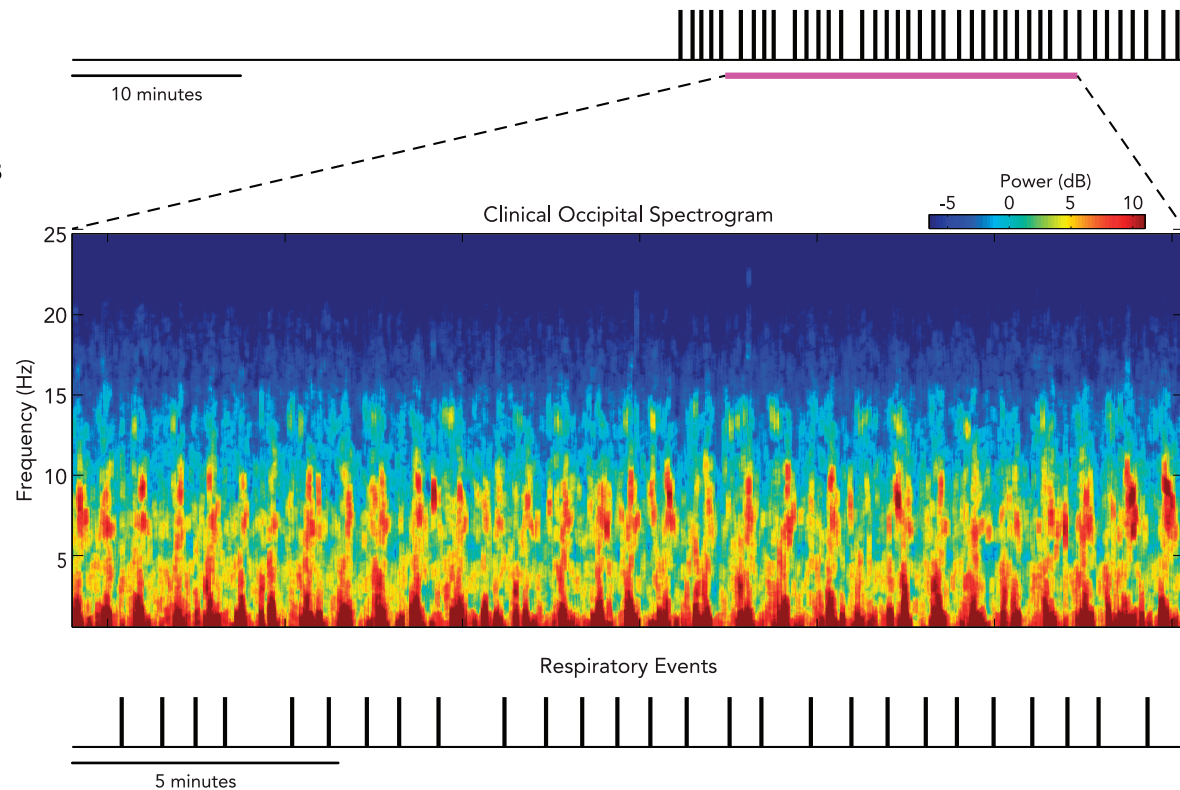
A**B**

FIGURE 12. The multitaper spectrogram reveals extreme fragmentation of NREM during respiratory events

In A, the hypnogram (top) occipital clinical multitaper sleep EEG spectrogram (middle) and the timing of technician-scored respiratory events (bottom) are shown for a subject with moderate to severe apnea (AHI: 27.9, RDI: 33.0). The multitaper spectrogram reveals a dramatic change during a series of respiratory (apnea and hypopnea) events occurring during NREM sleep. At the onset of the respiratory events, the low-frequency power typical of NREM becomes highly fragmented, with suppression and coincident reappearance of power in delta/theta, alpha, and sigma at each event.

work for objectively phenotyping sleep as a function of oscillatory dynamics. We believe that this approach holds great promise for advancing clinical sleep medicine and sleep research.

These quantitative benefits suggest several major practical advantages of a multitaper spectral approach to sleep EEG analysis. Clinically, the multitaper spectrogram provides an easy and powerful way to characterize a whole night of sleep dynamics in a single view, with a resolution that enables detailed analysis down to the microevent level. Thus the multitaper spectrogram could facilitate or replace traditional R&K methods by providing a way to rapidly identify spectral motifs for visual or automated staging of sleep. Inspection of the full-night multitaper spectrogram alone could be used to provide an initial rapid assessment of overall sleep architecture and fragmentation, as well as a means of triaging more time-consuming or costly subsequent analyses. There are also clinical scenarios such as split night studies and multiple sleep latency tests (MSLT) in which sleep staging and/or total sleep time (TST) must be estimated on the fly. The results of our spectral scoring experiment suggest that the multitaper EEG spectrogram could provide a clinically equivalent basis for estimating TST in these scenarios, the accuracy of which could be even further improved by including additional signals from the PSG. Furthermore, the ability to effortlessly identify clear features of sleep microstructure not captured in traditional scoring (i.e., spindles, K-complexes, peri-REM alpha bursts, etc.) greatly expands the set of potentially clinically relevant features to explore.

From a basic research standpoint, the multitaper spectrogram could provide a vital link between animal and human studies. Currently, it is not always possible to establish definitive equivalence between human sleep neurophysiology and the networks and cell-types explored in animal studies. This is because the vast preponderance of our knowledge of human sleep comes from analysis of cortical activity through EEG, whereas the knowledge gained from animal studies illuminates subcortical mechanisms. While intracranial recording is possible in certain clinical populations, these studies are difficult to undertake, involving patients with severe disorders (e.g., refractory epilepsy). Moreover, it is generally infeasible to probe certain regions of human neuroanatomy (e.g., the brain stem). Other imaging methods such as functional magnetic resonance imaging (fMRI) or magnetoencephalography (MEG) offer excellent spatial or temporal resolution but are costly and are not conducive of sleep. Thus, for the moment, EEG is the least invasive, least expensive, least disruptive, highest temporal resolution method for

measuring neurophysiological activity in sleeping humans. We believe that the multitaper spectrogram analysis provides an ideal means to characterize EEG data and relate it to possible underlying neural mechanisms. For example, Chervin et al. (23) explored the relationship between respiratory cycle-related spectral features of the human EEG to predict OSA-related sleepiness, whereas Tartar et al. (92) showed apnea-like sleep interruption caused an impairment of long-term potentiation (LTP), a synaptic correlate of learning and memory, in rodents. Further study of the broadband effects observed in the multitaper spectrogram (FIGURE 12) could therefore help elucidate the mechanisms and effects of OSA on the human brain, and distinguish sub-phenotypes that might account for heterogeneous symptomatic manifestations of OSA clinically.

Furthermore, given the link between the sleep EEG and the underlying neural mechanisms, the multitaper spectrogram could be used to provide deeper phenotyping of sleep dynamics and oscillation characteristics in healthy subjects as well as in clinical populations. There is a wealth of data now available regarding changes in EEG oscillations in a plethora of sleep disorders, as well as psychiatric and neurological disease states. Use of the multitaper spectrogram could make it possible to discern differences between healthy and disease states that are impossible to see using the hypnogram alone. Therefore, we encourage further use of this method in sleep research, particularly in neurological and psychiatric problems known to disturb sleep.

There are several technical enhancements that could further improve this proposed methodology. In this work, we have shown that all major R&K features of the sleep EEG can be observed within a single occipital multitaper spectrogram. At the same time, in our experimental data figures, we used a combination of occipital and central electrodes, which, in our experience enhances the clarity of the resulting sleep EEG spectrograms. More generally, given the circuit-specific localization of sleep processes within the brain (52, 66, 97), this approach could be made even more informative by utilizing spatial information in multi-channel or high-density EEG measurements. Additionally, we thus far have illustrated the application of the multitaper spectrogram to sleep EEG characterization in a qualitative manner. This approach, however, provides a rich framework for quantitative analyses of sleep states and characteristics. To those ends, future studies could leverage recent work that has developed signal processing techniques for tracking the nonstationary dynamics of many simultaneous neural oscillations within the multitaper spectrogram (74) or state-space methods

for modeling the changes in the oscillations as a function of sleep state (73). Overall, the multitaper spectrogram provides an objective, high-resolution, statistically efficient basis for powerful analyses, which could help to further illuminate the mechanisms of the sleeping brain. ■

APPENDIX

Spectral Estimation Techniques.

In this section, we describe the most common methods for spectral estimation, and the moti-

vating factors for the multitaper method. For a detailed overview of spectral estimation and the multitaper method, see Babadi and Brown (13).

The most common method of spectral estimation is the periodogram, which uses the discrete Fourier transform (33, 46) as the basis of spectral decomposition. For a random signal x_k , sampled at intervals of Δt where $k = 0, \dots, N - 1$, $\hat{S}_p(f)$, the periodogram at frequency f is defined as

$$\hat{S}_p(f) = \Delta t \left| \sum_{k=0}^{N-1} x_k e^{2\pi k f \Delta t} \right|^2. \quad (3)$$

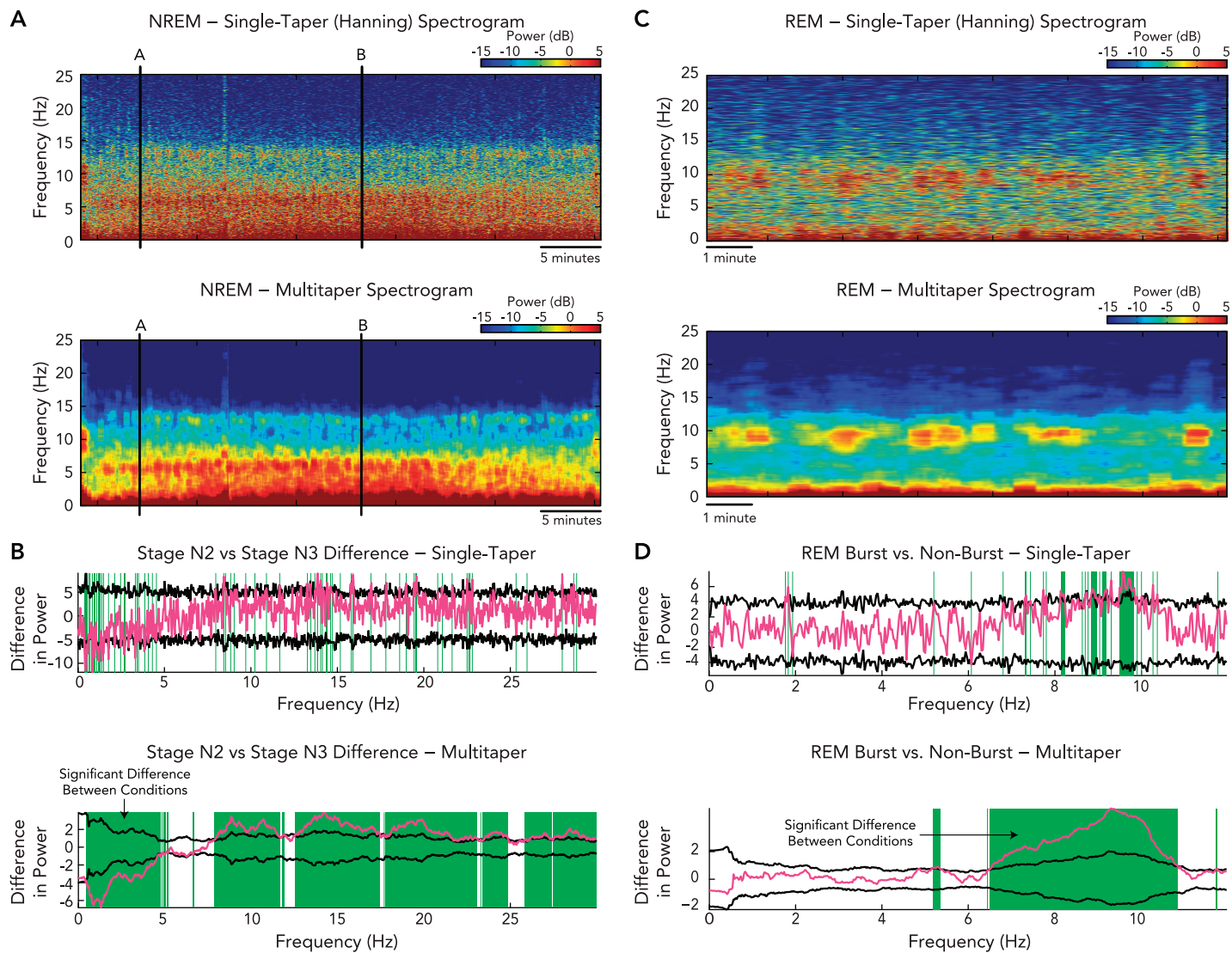


FIGURE 13. The multitaper spectrogram quantitatively characterizes changes in sleep state that are too subtle to detect using the single-taper spectrogram

A: the single-taper (Hanning) (top) and multitaper (bottom) spectrograms were computed for a single channel of occipital EEG during NREM, from which the spectra were extract from 2-min segments around early (marker A) and late (marker B) stage N2 sleep. **B:** a global acceptance bounds analysis of the single-taper spectrogram (top) showed no significant differences (green regions) between the two time periods, whereas the same analysis on the multitaper spectra (bottom) showed significant differences in frequency content in delta, alpha, sigma, and gamma power. **C:** in a second analysis, the single-taper (Hanning) (top) and multitaper (bottom) spectrograms were computed for a single channel of occipital EEG during REM, from which the spectra were extract from peri-REM burst times and non-burst times. **D:** a global acceptance bounds analysis of the single-taper spectrogram (top) shows no significant differences (green regions) between the burst and non-burst spectra, whereas the same analysis on the multitaper spectra (bottom) showed significant differences in frequency content low-alpha power. In these analyses, the observed difference in spectral power (magenta curves) is compared with global acceptance bands (black curves) constructed using the procedures outlined in Ref. 35. Contiguous points at which the observed spectral difference exceeds the global bounds are considered significantly different.

Because of the finite duration of experimentally observed signals, the periodogram suffers from two potential problems. First, the spectral estimate is biased; i.e., on average, the periodogram will be different from the true underlying spectrum. The consequence of this bias is that peaks within the spectrum can appear less distinct and blurred across frequencies. In addition, the periodogram has high variance due to the fact that the data are a single realization of a random signal. This produces noisy estimates of the spectrum.

In an effort to reduce the estimate bias, a common technique is to apply a taper or a window to the data. Common tapers used are Welch, Hanning, and Hamming functions, which tend to limit the amount of bias or blurring. $\hat{S}_{stp}(f)$, the single-tapered periodogram at frequency f is defined as

$$\hat{S}_{stp}(f) = \Delta t \left| \sum_{k=0}^{N-1} w_k x_k e^{2\pi kf\Delta t} \right|^2, \quad (4)$$

where w_k is the value of the taper at time k .

While the single-tapered spectral estimate reduces the estimation bias compared to the periodogram, the commonly used tapers are not optimal for bias reduction, and the variance of the spectral estimate is still high.

Multitaper spectral estimation (93) was designed to improve on the single-taper estimator by simultaneously addressing the issues of bias and variance, and does so by averaging the estimates from multiple tapers applied to the same data window, which are optimized to limit bias. These tapers are taken from a class of functions called the discrete prolate spheroid sequence (DPSS), also known as the Slepian sequence. These functions are designed to optimize the concentration of power in the main lobe with respect to the rest of the function, such that, for a taper W

$$\max_W \left[\frac{\text{power in the main lobe}}{\text{total power}} \right]. \quad (5)$$

This is referred to as solving the spectral concentration problem. It turns out that optimizing for main lobe power concentration (which involves eigenfunctions) produces tapers that are orthogonal, meaning they each extract independent estimates of the spectrum from the same window of data. In doing so, multiple estimates with reduced bias can be averaged together to produce a single estimate of the spectrum with reduced bias and variance.

The choice of $L = \lfloor 2TW \rfloor - 1$ for the number of tapers (Eq. 2) is based on the fact that the benefit of adding a taper drops precipitously when the number of tapers reaches a quantity known as the Shannon number, which in this case happens to be equal to $2TW$ (69). Thus, by setting the number of tapers to one less than this quantity, we can produce an efficient estimate that uses no more than the maximum number of significant tapers.

Given a set of L DPSS tapers $\{w^1, \dots, w^L\}$, $\hat{S}_{mt}(f)$, the multitaper spectral estimate at frequency f is defined as

$$\hat{S}_{mt}(f) = \frac{1}{L} \sum_{l=1}^L \left| \sum_{k=0}^{N-1} w_k^l x_k e^{2\pi kf\Delta t} \right|^2, \quad (6)$$

in which the spectral estimate is the average of the single-taper estimates for each taper. It can be shown (7) that the multitaper estimate reduces the variance by a factor of approximately L compared with single-tapered estimates.

Quantitative Advantages of Multitaper Spectral Analysis

To establish the quantitative improvement of the multitaper spectrogram over the single-taper spec-

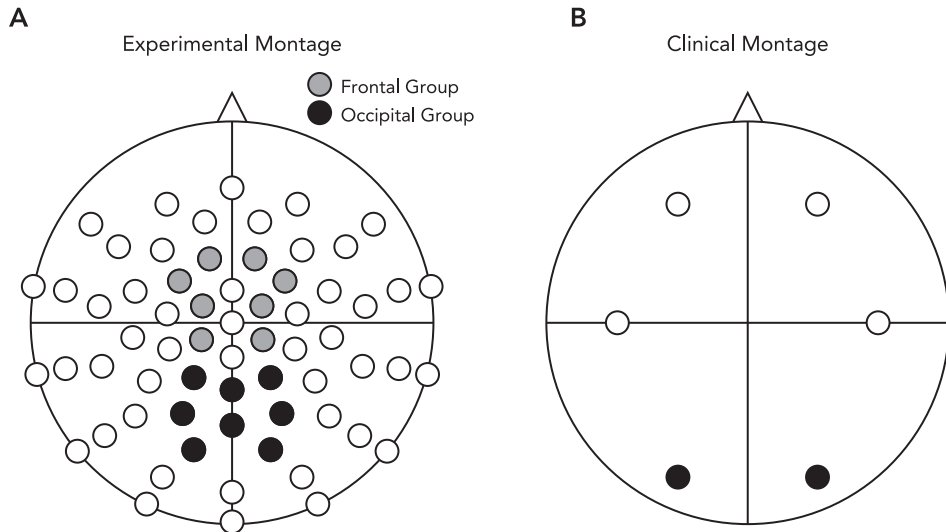


FIGURE 14. The experimental (A) and clinical (B) EEG electrode montages used for spectral estimation

rogram, we performed an analysis testing the ability of each method to distinguish differences in the sleep EEG between two meaningful contexts. To do so, we employed an established procedure (35) for detecting significant regions of difference in multidimensional data by constructing global acceptance bounds for hypothesis testing. Given two sets of spectra from different conditions, the method constructs a null distribution on the mean difference between groups by repeatedly permuting the conditions labels and generating the mean difference between sets at each iteration. Given this null distribution, the method constructs global acceptance bounds (FIGURE 13, black curves) by finding the region that completely contains 95% of the permuted means across every single frequency. By doing so, the method controls the family-wise error rate (FWER), and thus every frequency at which the observed difference between the two conditions falls outside of these global bounds is considered significant. Contiguous significant frequencies are thus considered regions of significance.

Using this procedure, we assessed the degree with which the single-taper (Hanning) and multitaper spectrogram could distinguish between changes in spectral power occurring during the transition from NREM Stage N2 sleep to Stage N3 sleep (FIGURE 13, A AND B). We first estimated single-taper (FIGURE 13A, TOP) and multitaper (FIGURE 13A, BOTTOM) spectrograms for a single channel of occipital EEG during NREM. For each spectrogram, we performed the global confidence analysis comparing the difference between spectra drawn from 2-min segments around a time point in Stage N2 sleep (*marker A*) and from another time point in Stage N3 sleep (*marker B*). In this case, the multitaper spectrogram was able to detect differences in sleep state that are indistinguishable from the single-taper spectrogram. The global acceptance analysis of the single-taper spectrogram (FIGURE 13B, TOP) showed no major contiguous regions of significance (green regions) between the two time periods, whereas the same analysis on the multitaper spectra (FIGURE 13B, BOTTOM) showed clear regions of significance in frequency content in delta, alpha, sigma, and gamma power.

We also assessed the degree with which single-taper and multitaper spectrogram could identify microevents during REM (FIGURE 13, C AND D). We proceeded as in the NREM analysis, estimating single-taper (FIGURE 13C, TOP) and multitaper (FIGURE 13C, BOTTOM) spectrograms for a single channel of occipital EEG during REM, from which times containing peri-REM alpha bursting were compared with non-burst times. Again, the multitaper spectrogram was able to detect differences in

sleep state that are indistinguishable from the single-taper spectrogram. The global acceptance analysis of the single-taper spectrogram (FIGURE 13D, TOP) showed no major contiguous regions of significance (green regions) between the two time periods, whereas the same analysis on the multitaper spectra (FIGURE 13D, BOTTOM) showed clear regions of significance in frequency content in the alpha range in which the bursting occurs.

These analyses therefore rigorously demonstrate the ability of the multitaper to discern the difference between EEG events too subtle to detect using traditional single-taper methods.

Electrode Montages for Spectral Estimation

FIGURE 14 shows the electrode montages used to construct the experimental and clinical sleep EEG spectrograms. The experimental data were recorded using a 64-channel Brain Vision system with Laplacian referencing (FIGURE 14A). The experimental spectrograms (excluding the single-channel examples) are the median spectrogram from the frontal (light gray) or occipital (dark gray) electrodes. The clinical data were recorded using a standard clinical setup with contralateral mastoid referencing, as per AASM standards (FIGURE 14B). Clinical spectrograms are the median of the two occipital channels.

The authors have developed a companion series of interactive online tutorials for this review at sleepeeg.org.

This work was supported by VA and by National Institutes of Health (NIH) Grants R21 NS-093000 (R.E.B.), R01 MH-039683 and HL-095491(R.E.B), National Institute Of Neurological Disorders And Stroke Grant R01 NS-096177 (M.J.P.), and by NIH New Innovator Award DP2-OD006454 (P.L.P.).

M.T.B. receives funding from the Department of Neurology, Massachusetts General Hospital, the Center for Integration of Medicine and Innovative Technology, the Milton Family Foundation, and the MGH-MIT Grand Challenge. M.T.B. has a pending patent on a sleep wearable device, received travel funds from Servier, served on the advisory board of Foramis, received research funding from MC10, Inc. and Insomnisolv, Inc., has consulting agreements with McKesson and with International Flavors and Fragrances, and has provided expert testimony in sleep medicine.

M.J.P. and P.L.P. have patents pending on the monitoring of sleep and anesthesia. M.T.B. has a patent pending for a sleep monitoring device.

Author contributions: M.J.P. drafted manuscript; M.J.P., P.L.P., R.E.B., M.T.E edited and revised manuscript; M.J.P., P.L.P., R.E.B., M.T.E, J.M.E approved final version of manuscript; M.J.P. and P.L.P. conceived and designed the research. M.J.P. performed the analyses. M.J.P., P.L.P., M.T.B., J.M.E. interpreted the results.

References

1. Adamantidis AR, Zhang F, Aravanis AM, Deisseroth K, De Lecea L. Neural substrates of awakening probed with optogenetic control of hypocretin neurons. *Nature* 450: 420–424, 2007.
2. Adrian E, Matthews BH. The Berger rhythm: potential changes from the occipital lobes in man. *Brain* 57: 355–385, 1934.

3. Adrian ED, Yamagiwa K. The origin of the Berger rhythm. *Brain* 58: 323–351, 1935.
4. Aserinsky E, Kleitman N. Regularly occurring periods of eye motility, and concomitant phenomena, during sleep. *Science* 118: 273–274, 1953.
5. Astori S, Wimmer RD, Luthi A. Manipulating sleep spindles: expanding views on sleep, memory, and disease. *Trends Neurosci* 36: 738–748, 2013.
6. Astori S, Wimmer RD, Prosser HM, Corti C, Corsi M, Liaudet N, Volterra A, Franken P, Adelman JP, Luthi A. The Ca(V)3.3 calcium channel is the major sleep spindle pacemaker in thalamus. *Proc Natl Acad Sci USA* 108: 13823–13828, 2011.
7. Babadi B, Brown EN. A review of multitaper spectral analysis. *IEEE Trans Biomed Eng* 61: 1555–1564, 2014.
9. Berger H. Über das Elektrenkephalogramm des Menschen. *Arch Psychiatr Nervenkr* 87: 527–570, 1929.
10. Bódizs R, Körmendi J, Rigó P, Lázár AS. The individual adjustment method of sleep spindle analysis: methodological improvements and roots in the fingerprint paradigm. *J Neurosci Methods* 178: 205–213, 2009.
11. Bollimunta A, Mo J, Schroeder CE, Ding M. Neuronal mechanisms and attentional modulation of corticothalamic alpha oscillations. *J Neurosci* 31: 4935–4943, 2011.
12. Bronez T. On the performance advantage of multitaper spectral analysis. *IEEE Trans Signal Proc* 40: 2941–2946, 1992.
13. Brown RE, Basheer R, McKenna JT, Strecker RE, McCarley RW. Control of sleep and wakefulness. *Physiol Rev* 92: 1087–1187, 2012.
15. Cantero JL, Atienza M. Alpha burst activity during human REM sleep: descriptive study and functional hypotheses. *Clin Neurophysiol* 111: 909–915, 2000.
16. Cantero JL, Atienza M, Salas RM. Human alpha oscillations in wakefulness, drowsiness period, and REM sleep: different electroencephalographic phenomena within the alpha band. *Neurophysiol Clin* 32: 54–71, 2002.
17. Cantero JL, Atienza M, Salas RM. Spectral features of EEG alpha activity in human REM sleep: two variants with different functional roles? *Sleep* 23: 746–750, 2000.
18. Cantero JL, Atienza M, Salas RM, Gomez C. Alpha power modulation during periods with rapid oculomotor activity in human REM sleep. *Neuroreport* 10: 1817–1820, 1999.
19. Cantero JL, Atienza M, Salas RM, Gomez CM. Brain spatial microstates of human spontaneous alpha activity in relaxed wakefulness, drowsiness period, and REM sleep. *Brain Topogr* 11: 257–263, 1999.
20. Cantero JL, Atienza M, Stickgold R, Kahana MJ, Madsen JR, Kocsis B. Sleep-dependent theta oscillations in the human hippocampus and neocortex. *J Neurosci* 23: 10897–10903, 2003.
21. Cardin JA, Carlen M, Meletis K, Knoblich U, Zhang F, Deisseroth K, Tsai LH, Moore CI. Driving fast-spiking cells induces gamma rhythm and controls sensory responses. *Nature* 459: 663–667, 2009.
22. Cash SS, Halgren E, Dehghani N, Rossetti AO, Thesen T, Wang C, Devinsky O, Kuzniecky R, Doyle W, Madsen JR, Bromfield E, Eross L, Halasz P, Karmos G, Csarcza R, Wittner L, Ulbert I. The human K-complex represents an isolated cortical down-state. *Science* 324: 1084–1087, 2009.
23. Chervin RD, Burns JW, Ruzicka DL. Electroencephalographic changes during respiratory cycles predict sleepiness in sleep apnea. *Am J Respir Crit Care Med* 171: 652–658, 2005.
24. Cirelli C, Tononi G. The search for the molecular correlates of sleep and wakefulness. *Sleep Med Rev* 5: 397–408, 2001.
25. Crunelli V, Hughes SW. The slow (<1 Hz) rhythm of non-REM sleep: a dialogue between three cardinal oscillators. *Nat Neurosci* 13: 9–17, 2010.
26. Datta S. Cellular basis of pontine ponto-geniculo-occipital wave generation and modulation. *Cell Mol Neurobiol* 17: 341–365, 1997.
27. De Gennaro L, Ferrara M. Sleep spindles: an overview. *Sleep Med Rev* 7: 423–440, 2003.
28. De Gennaro L, Ferrara M, Vecchio F, Curcio G, Bertini M. An electroencephalographic fingerprint of human sleep. *Neuroimage* 26: 114–122, 2005.
29. Dehghani N, Cash SS, Halgren E. Topographical frequency dynamics within EEG and MEG sleep spindles. *Clin Neurophysiol* 122: 229–235, 2011.
30. Dement W, Kleitman N. The relation of eye movements during sleep to dream activity: an objective method for the study of dreaming. *J Exp Psychol* 53: 339–346, 1957.
31. Dijk DJ, Hayes B, Czeisler CA. Dynamics of electroencephalographic sleep spindles and slow wave activity in men: effect of sleep deprivation. *Brain Res* 626: 190–199, 1993.
- 31a. Donnelly D. The fast Fourier and Hilbert-Huang transforms: a comparison. In: *Computational Engineering in Systems Applications, IMACS Multi-conference*. New York: IEEE, 2006, p. 84–88.
32. Fernandez-Mendoza J, Lozano B, Seijo F, Santamaría-Liebana E, Ramos-Platón MJ, Vela-Bueno A, Fernandez-Gonzalez F. Evidence of subthalamic PGO-like waves during REM sleep in humans: a deep brain polysomnographic study. *Sleep* 32: 1117–1126, 2009.
33. Fourier JBJ. *Théorie Analytique de la Chaleur*. Cambridge, UK: Cambridge Univ. Press, 2009, p. 676.
34. Fraigne JJ, Torontali ZA, Snow MB, Peever JH. REM sleep at its core: circuits, neurotransmitters, and pathophysiology. *Front Neurol* 6: 123, 2015.
35. Fujisawa S, Amarasingham A, Harrison MT, Buzsaki G. Behavior-dependent short-term assembly dynamics in the medial prefrontal cortex. *Nat Neurosci* 11: 823–833, 2008.
36. Grigg-Damberger MM. The AASM scoring manual four years later. *J Clin Sleep Med* 8: 323–332, 2012.
37. Grigg-Damberger MM. The AASM scoring manual: a critical appraisal. *Curr Opin Pulm Med* 15: 540–549, 2009.
38. Halassa MM, Siegle JH, Ritt JT, Ting JT, Feng G, Moore CI. Selective optical drive of thalamic reticular nucleus generates thalamic bursts and cortical spindles. *Nat Neurosci* 14: 1118–1120, 2011.
39. Hori T, Hayashi M, Morikawa T. Topographical EEG changes and the hypnagogic experience. In: *Sleep Onset: Normal and Abnormal Processes*, edited by Ogilvie RD, Harsh JR. Washington, DC: Am. Psychological Association, 1994, p. 237–253.
40. Hughes SW, Crunelli V. Thalamic mechanisms of EEG alpha rhythms and their pathological implications. *Neuroscientist* 11: 357–372, 2005.
- 40a. Huang NE, Wu Z. A review on Hilbert-Huang transform: method and its applications to geophysical studies. *Rev Geophys* 46: RG2006, 2008.
41. Hughes SW, Lorincz M, Cope DW, Bleethyn KL, Kekesi KA, Parri HR, Juhasz G, Crunelli V. Synchronized oscillations at alpha and theta frequencies in the lateral geniculate nucleus. *Neuron* 42: 253–268, 2004.
42. Iber C, Ancoli-Israel S, Chesson Jr. AL, Quan SF. *The AASM Manual for the Scoring of Sleep and Associated Events: Rules, Terminology and Technical Specification*. Westchester, IL: Am. Acad. of Sleep Medicine, 2007.
43. Jahnsen H, Llinás R. Electrophysiological properties of guinea-pig thalamic neurones: an *in vitro* study. *J Physiol* 349: 205–226, 1984.
44. Jahnsen H, Llinás R. Ionic basis for the electroresponsiveness and oscillatory properties of guinea-pig thalamic neurones *in vitro*. *J Physiol* 349: 227–247, 1984.
45. Jones SR, Pritchett DL, Sikora MA, Stufflebeam SM, Hamalainen M, Moore CI. Quantitative analysis and biophysically realistic neural modeling of the MEG mu rhythm: rhythmogenesis and modulation of sensory-evoked responses. *J Neurophysiol* 102: 3554–3572, 2009.
46. Kammler DW. *A First Course in Fourier Analysis*. Cambridge, UK: Cambridge Univ. Press, 2008, p. 798.
47. Kim T, Thankachan S, McKenna JT, McNally JM, Yang C, Choi JH, Chen L, Kocsis B, Deisseroth K, Strecker RE, Basheer R, Brown RE, McCarley RW. Cortically projecting basal forebrain parvalbumin neurons regulate cortical gamma band oscillations. *Proc Natl Acad Sci USA* 112: 3535–3540, 2015.
48. Klimesch W. alpha-band oscillations, attention, and controlled access to stored information. *Trends Cogn Sci* 16: 606–617, 2012.
49. Kokkinos V, Koupparis A, Stavrinos ML, Kostopoulos GK. The hypnospectrogram: an EEG power spectrum based means to concurrently overview the macroscopic and microscopic architecture of human sleep. *J Neurosci Meth* 185: 29–38, 2009.
50. Koupparis AM, Kokkinos V, Kostopoulos GK. Semi-automatic sleep EEG scoring based on the hypnospectrogram. *J Neurosci Methods* 221: 189–195, 2014.
51. Krueger JM, Huang YH, Rector DM, Buysse DJ. Sleep: a synchrony of cell activity-driven small network states. *Eur J Neurosci* 38: 2199–2209, 2013.
52. Krueger JM, Rector DM, Roy S, Van Dongen HP, Belenky G, Panksepp J. Sleep as a fundamental property of neuronal assemblies. *Nat Rev Neurosci* 9: 910–919, 2008.
53. Lehtela L, Salmelin R, Hari R. Evidence for reactive magnetic 10-Hz rhythm in the human auditory cortex. *Neurosci Lett* 222: 111–114, 1997.
54. Lim AS, Lozano AM, Moro E, Hamani C, Hutchinson WD, Dostrovsky JO, Lang AE, Wennberg RA, Murray BJ. Characterization of REM-sleep associated ponto-geniculo-occipital waves in the human pons. *Sleep* 30: 823–827, 2007.
55. Limoges E, Mottron L, Bolduc C, Berthiaume C, Godbout R. Atypical sleep architecture and the autism phenotype. *Brain* 128: 1049–1061, 2005.
56. Loomis AL, Harvey EN, Hobart GA. Cerebral states during sleep, as studied by human brain potentials. *J Exp Psychol* 21: 127–144, 1937.
57. Lorincz ML, Crunelli V, Hughes SW. Cellular dynamics of cholinergically induced alpha (8–13 Hz) rhythms in sensory thalamic nuclei *in vitro*. *J Neurosci* 28: 660–671, 2008.
58. Lorincz ML, Kekesi KA, Juhasz G, Crunelli V, Hughes SW. Temporal framing of thalamic relay-mode firing by phasic inhibition during the alpha rhythm. *Neuron* 63: 683–696, 2009.
59. Magnin M, Rey M, Bastuji H, Guillemin P, Mau-guière F, Garcia-Larrea L. Thalamic deactivation at sleep onset precedes that of the cerebral cortex in humans. *Proc Natl Acad Sci USA* 107: 3829–3833, 2010.

60. Magosso E, Ursino M, Provini F, Montagna P. Wavelet analysis of electroencephalographic and electro-oculographic changes during the sleep onset period. *Conf Proc IEEE Eng Med Biol Soc* 2007: 4006–4010, 2007.
- 60a. Mandic DP, Rehman N, Wu Z, Huang NE. Empirical mode decomposition-based time-frequency analysis of multivariate signals: the power of adaptive data analysis. *IEEE Sign Proc Mag* 30: 74–86, 2013.
61. Manoach DS, Demanuele C, Wamsley E, Montrose D, Miewald J, Kupfer D, Buysse D, Stickgold R, Keshavan M. Sleep spindle deficits in early course, antipsychotic naïve patients with schizophrenia. In: *Society for Biological Psychiatry Annual Meeting Presentation*. Jacksonville, FL: Soc. of Biological Psychiatry, 2014, p. 913.
62. Manoach DS, Demanuele C, Wamsley EJ, Montrose D, Miewald J, Kupfer D, Buysse DJ, Stickgold R, Keshavan M. Sleep spindle deficit in first degree relatives of patients with schizophrenia. In: *Society for Biological Psychiatry Annual Meeting Presentation*. Jacksonville, FL: Soc. of Biological Psychiatry, 2014, p. 188.
63. Manoach DS, Demanuele C, Wamsley EJ, Vangel M, Montrose DM, Miewald J, Kupfer D, Buysse D, Stickgold R, Keshavan MS. Sleep spindle deficits in antipsychotic-naïve early course schizophrenia and in non-psychotic first-degree relatives. *Front Hum Neurosci* 8: 762, 2014.
64. Mo J, Schroeder CE, Ding M. Attentional modulation of alpha oscillations in macaque inferotemporal cortex. *J Neurosci* 31: 878–882, 2011.
65. Nalatore H, Rangarajan G. Short-window spectral analysis using AMVAR and multitaper methods: a comparison. *Biol Cybern* 101: 71–80, 2009.
66. Nir Y, Staba RJ, Andrillon T, Vyazovskiy VV, Cirelli C, Fried I, Tononi G. Regional slow waves and spindles in human sleep. *Neuron* 70: 153–169, 2011.
67. Ogilvie RD. The process of falling asleep. *Sleep Med Rev* 5: 247–270, 2001.
68. Palva S, Palva JM. New vistas for alpha-frequency band oscillations. *Trends Neurosci* 30: 150–158, 2007.
69. Percival DB, Walden AT. *Spectral Analysis for Physical Applications: Multitaper and Conventional Univariate Techniques*. Cambridge, UK: Cambridge Univ. Press, 1993.
70. Percival DB, Walden AT. *Wavelet Methods for Time Series Analysis*. Cambridge, UK: Cambridge Univ. Press, 2000.
71. Pigorini A, Casali AG, Casarotto S, Ferrarelli F, Baselli G, Mariotti M, Massimini M, Rosanova M. Time-frequency spectral analysis of TMS-evoked EEG oscillations by means of Hilbert-Huang transform. *J Neurosci Methods* 198: 236–245, 2011.
72. Pracka T, Pracka D, Ziołkowska-Kochan M. The modified color density spectral array: an alternative method for sleep presentation. *Acta Neurobiol Exp (Warsz)* 68: 516–518, 2008.
73. Prerau MJ, Hartnack KE, Obregon-Henao G, Sampson A, Merlino M, Gannon K, Bianchi MT, Ellenbogen JM, Purdon PL. Tracking the sleep onset process: an empirical model of behavioral and physiological dynamics. *PLoS Comput Biol* 10: e1003866, 2014.
74. Prerau MJ, Purdon PL, Eden UT. Tracking non-stationary spectral peak structure in EEG data. *Conf Proc IEEE Eng Med Biol Soc* 2013: 417–420, 2013.
75. Priestley MB. *Spectral Analysis and Time Series*. London: Academic, 1981.
76. Ray LB, Fogel SM, Smith CT, Peters KR. Validating an automated sleep spindle detection algorithm using an individualized approach. *J Sleep Res* 19: 374–378, 2010.
77. Rechtschaffen A, Kales A. *A Manual of Standardized Terminology, Techniques, and Scoring Systems for Sleep Stages of Human Subjects*. Washington, DC: Public Health Service, 1968.
78. Salinsky M, Goins S, Sutula T, Roscoe D, Weber S. Comparison of sleep staging by polygraph and color density spectral array. *Sleep* 11: 131–138, 1988.
79. Salinsky M, Sutula T, Roscoe D. Representation of sleep stages by color density spectral array. *Electroencephalogr Clin Neurophysiol* 66: 579–582, 1987.
80. Santamaria J, Chiappa KH. The EEG of drowsiness in normal adults. *J Clin Neurophysiol* 4: 327–382, 1987.
81. Sasaki K, Suzuki M, Mieda M, Tsujino N, Roth B, Sakurai T. Pharmacogenetic modulation of orexin neurons alters sleep/wakefulness states in mice. *PLoS One* 6: e20360, 2011.
82. Shibagaki M, Kiyono S, Watanabe K. Spindle evolution in normal and mentally retarded children: a review. *Sleep* 5: 47–57, 1982.
83. Silber MH, Ancoli-Israel S, Bonnet MH. The visual scoring of sleep in adults. *J Clin Sleep* 3: 121–131, 2007.
84. Silva LR, Amitai Y, Connors BW. Intrinsic oscillations of neocortex generated by layer 5 pyramidal neurons. *Science* 251: 432–435, 1991.
85. Slepian D. Prolate spheroidal wave functions, Fourier analysis, and uncertainty-V: the discrete case. *Bell Sys Tech J* 57: 1371–1430, 1978.
86. Sohal VS, Zhang F, Yizhar O, Deisseroth K. Parvalbumin neurons and gamma rhythms enhance cortical circuit performance. *Nature* 459: 698–702, 2009.
87. Steriade M, Amzica F, Nuñez A. Cholinergic and noradrenergic modulation of the slow (approximately 0.3 Hz) oscillation in neocortical cells. *J Neurophysiol* 70: 1385–1400, 1993.
88. Steriade M, Contreras D, Curro DR, and Nuñez A. The slow (< 1 Hz) oscillation in reticular thalamic and thalamocortical neurons: scenario of sleep rhythm generation in interacting thalamic and neocortical networks. *J Neurosci* 13: 3284–3299, 1993.
89. Steriade M, McCarley RW. *Brain Control of Wakefulness and Sleep*. New York: Plenum, 2005.
90. Steriade M, Nuñez A, Amzica F. Intracellular analysis of relations between the slow (<1 Hz) neocortical oscillation and other sleep rhythms of the electroencephalogram. *J Neurosci* 13: 3266–3283, 1993.
91. Steriade M, Nuñez A, Amzica F. A novel slow (< 1 Hz) oscillation of neocortical neurons in vivo: depolarizing and hyperpolarizing components. *J Neurosci* 13: 3252–3265, 1993.
92. Tartar JL, Ward CP, McKenna JT, Thakkar M, Arrigoni E, McCarley RW, Brown RE, Strecker RE. Hippocampal synaptic plasticity and spatial learning are impaired in a rat model of sleep fragmentation. *Eur J Neurosci* 23: 2739–2748, 2006.
93. Thomson DJ. Spectrum estimation and harmonic analysis. *Proc IEEE* 70: 1055–1096, 1982.
94. van Vugt MK, Sederberg PB, Kahana MJ. Comparison of spectral analysis methods for characterizing brain oscillations. *J Neurosci Methods* 162: 49–63, 2007.
95. Vassalli A, Dellepiane JM, Emmenegger Y, Jimenez S, Vandi S, Plazzi G, Franken P, Tafti M. Electroencephalogram paroxysmal theta characterizes cataplexy in mice and children. *Brain* 136: 1592–1608, 2013.
96. Vertes RP, Kocsis B. Brainstem-diencephalo-septohippocampal systems controlling the theta rhythm of the hippocampus. *Neuroscience* 81: 893–926, 1997.
97. Vyazovskiy VV, Olcese U, Hanlon EC, Nir Y, Cirelli C, Tononi G. Local sleep in awake rats. *Nature* 472: 443–447, 2011.
98. Wamsley EJ, Tucker MA, Shinn AK, Ono KE, McKinley SK, Ely AV, Goff DC, Stickgold R, Manoach DS. Reduced sleep spindles and spindle coherence in schizophrenia: mechanisms of impaired memory consolidation? *Biol Psychiatry* 71: 154–161, 2012.
99. Warby SC, Wendt SL, Welinder P, Munk EG, Carrillo O, Sorensen HB, Jennum P, Peppard PE, Perona P, Mignot E. Sleep-spindle detection: crowdsourcing and evaluating performance of experts, non-experts and automated methods. *Nat Methods* 11: 385–392, 2014.
100. Welch PD. The use of fast Fourier transform for the estimation of power spectra: a method based on time averaging over short, modified periodograms. *IEEE Trans Audio Electroacoust* 15: 70–73, 1967.
101. Werth E, Achermann P, Dijk DJ, Borbély AA. Spindle frequency activity in the sleep EEG: individual differences and topographic distribution. *Electroencephalogr Clin Neurophysiol* 103: 535–542, 1997.
102. Xie L, Kang H, Xu Q, Chen MJ, Liao Y, Thiagarajan M, O'Donnell J, Christensen DJ, Nicholson C, Iliff JJ, Takano T, Deane R, Nedergaard M. Sleep drives metabolite clearance from the adult brain. *Science* 342: 373–377, 2013.